

Ignition and Combustion Characteristics of Overloaded Wire Insulations Under Weakly Buoyancy or Microgravity Environments



Wenjun Kong, Kai Wang, Wei Xia and Shao Xue

Abstract The electric wire, cable and components are the potential igniters, which might cause fire under certain unexpected circumstances. This chapter focuses on the pre-ignition characteristics by overload, the soot emission from the wire insulation during the pre-ignition and ignition stages, the smoke release and distribution characteristics of wire insulation combustion. We reviewed the research work on wire insulations completed by the authors. We first presented the functional simulation methods. The concept of “function simulation” means that the simulation is satisfied in heat transfer sense. A low pressure narrow channel method (LPNCM) was proposed to study fire initiation of wire insulation at microgravity. Then we introduced the experiments completed in microgravity by using the China recoverable satellites of SJ-8 and SJ-10. The experimental hardware were developed to perform the experiments of wire insulation experiments caused by overload on board the SJ-8 and SJ-10 China recoverable satellites, respectively. In the experiments, the pre-fire characteristics including the temperature and radiation characteristics of the wire insulations were presented. For the SJ-10 experiments, the smoke emissions of overloaded wires insulations were investigated. Two smoke emitting modes, namely the end smoke jet and the bubbling smoke jet were identified with polyethylene insulation. The results show that the morphology of pyrolysis front dominated the direction and the range of the end smoke jet. The effects of the insulation thickness and the excess current on the temperature rise were discussed.

Keywords Fire safety · China recoverable satellites · Wire insulation · Function simulation · Overload

W. Kong (✉) · K. Wang · W. Xia · S. Xue
Institute of Engineering Thermophysics, Chinese Academy of Sciences, University of Chinese Academy of Sciences, Beijing, China
e-mail: wjkong@buaa.edu.cn

W. Kong
Beihang University, Beijing, China

K. Wang
Commercial Aircraft Engine Co., Ltd., Aero Engine Corporation of China, Shanghai, China

© Science Press and Springer Nature Singapore Pte Ltd. 2019
W. R. Hu and Q. Kang (eds.), *Physical Science Under Microgravity: Experiments on Board the SJ-10 Recoverable Satellite*, Research for Development,
https://doi.org/10.1007/978-981-13-1340-0_9

1 Introduction

Fire safety is one of the most important problems which must be solved properly for the manned space flight since it is closely related to the safety of astronauts and the success of the flight mission.

The well-known fire triangle shows that combustible materials (non-metallic materials), oxygen and igniter are the three necessary elements for fire. Although each one of the three elements is equally important the experiences of manned space flight show that the igniter made much trouble frequently as shown in Table 1 [1]. At least five fire-threatening incidents (STS-6, STS-28, STS-35, STS-40, STS-50) have been reported in the first 50 missions of the US Space Shuttle since 1981. The fire-risk probability is 10%.

Table 1 Shuttle fire-risk experience

| Mission | Date | Incident | Result | Response |
|---------|---------------|---|--|--|
| STS-6 | April 1983 | Wires fused near material processing unit; crew detected an odor | No atmospheric contamination measured | No alarm |
| STS-28 | August 1989 | Cable strain at connector to teleprinter caused insulation failure and electrical short circuit; crew detected a few embers and smoke | Smoke and particle concentration recorded | Circuit breaker did not open; no alarm |
| STS-35 | December 1990 | Overheated resistor in digital display unit; crew detected an odor | No atmospheric contamination measured | No alarm |
| STS-40 | June 1991 | Refrigerator-freezer fan motor failed; crew noted an irritating odor | Atmospheric contamination identified post-flight | No alarm |
| STS-50 | June 1992 | Electronic capacitor in negative body pressure apparatus failed; crew detected an odor | No atmospheric contamination measured | No alarm |

These five fire-threatening incidents are all involved electrical component overheating or electrical short circuits [2, 3]. Heat and increasing temperature due to overload contribute to produce fire. Thus, the electric wire, cable and components are the potential igniters it might cause fire under certain unexpected circumstances.

In order to eliminate these potential igniters as much as possible a series of extremely strict qualification tests have been setup. But all these tests have been conducted on the ground, the microgravity effects were not fully taken into account. Since the natural convection almost vanished at microgravity, the heat transfer of the electric components is quite different at microgravity from on the ground, due to the significantly suppressed natural convection, leading to more heat accumulation in the vicinity of electrical wires and components and higher wire insulation temperatures. The heat loss of the electric components decreased, it might cause the overheating of the electric components and then results in fire. Consequently, it is much more likely to encounter fire threatening scenarios in microgravity due to overheating of electrical wires or components under overload conditions. Therefore, the overheating and damage of wire insulation is one of the main sources of fire incident during manned spacecraft flights.

The ignition of wire insulation by overload in normal atmosphere and gravity has been extensively investigated, with the modes of ignition being classified as (1) arcing, (2) excessive Ohmic heating, and (3) ignition from external heating, and possible contributing factors to ignition systematically discussed [4]. However, there have been limited studies on the ignition of wire insulation in microgravity. The thermal ignition of wire insulation under overload conditions is a slow process, which could take several minutes, several hours, or even longer. It is impossible to create such a long microgravity duration on the ground. Besides, the ground-based tests were limited to very thin fuels, like tissue paper. Practical combustible materials, such as the wire insulation, are thicker and require much longer test time than what is available [5]. On the other hand, space flight experiments in the real microgravity environment are very expensive and not realistic to be conducted on a regular basis.

Anyway, in previous microgravity fire accidents, the fire monitoring and alarm devices did not work, but crew discovered it after they detected an odor or smoke. Based on these, NASA and ESA agreed to strengthen basic research on ignition symptoms in microgravity environments. NASA has funded microgravity research projects to study the combustion characteristics of wire insulations.

Thomas and Donald [6] conducted the first research on the combustion of wire insulations in microgravity in 1971. They found that the Teflon wire insulation could be ignited in 5 s under microgravity in a drop tower. Later, Greenberg et al. [5, 7] provided results of opposed and concurrent flame spreading over polyethylene-insulated nichrome wires by using the Space Shuttle. It was difficult to investigate all the parameters that influence the combustion characteristics of wire insulation, such as oxygen concentration, initial wire temperature, wire diameter, ambient pressure, and dilution gas, because of the limited number of experiments. Kikuchi et al. [8, 9] and Fujita et al. [10, 11] reported results on flame spreading over preheated wire in a quiescent atmosphere in microgravity and investigated the effect of oxygen concentration, dilution gas, wire preheating, and wire thickness by using

the 10 s drop tower. Umem et al. [12] proposed a mathematical model to describe the combustion characteristics of ETFE-coated copper wire in microgravity.

We know electrical wires can be involved in a fire by either being subjected to an external heat source or being subjected to internal heating. All above mentioned works conducted by the US and Japan counterparts, only external ignition sources leading to flame spread along wire surface were investigated. In these works, the wire insulation was firstly preheated by electrical overload to a predetermined temperature and then terminated the wire heating and activated the ignitor to produce the flame spreading over the insulation. It is similar to study on flame spread along fuel cylinders, and the results, in fact, cannot fully explain the phenomenon of fire caused by the wire overload and fatigue in microgravity, especially the ignition premonition of the electrical components cannot be obtained. One has to pay much more attentions to study the wire insulations damage by the current overload. It is the most cases of fire involved in wires in microgravity. The understandings of the ignition premonition of wire insulation involved in a fire by being subjected to internal heating has practical signification on the development of fire-prevention measures in manned spacecraft.

Based to our literature search, the combustion characteristics of wire insulation caused by the overload and fatigue of the electrical components in microgravity or weakly buoyant environment were first investigated by the authors here [13–16]. A “function simulation” method [13–15] was proposed and a long time microgravity experiment was conducted on board of the SJ-8 China recoverable satellites in 2006 to study the pre-ignition temperature variations of wire insulations [16].

Nakamura et al. [17, 18] also studied the flame spread of wire insulations in low pressure and showed that the microgravity effect could be simulated by low pressure environment on the ground. After that, Fujita et al. [19] and Takano et al. [20] investigated the flammability of wire insulations by overload with drop tower. These works showed that ignition of wire insulation by current overload was quite a different process in microgravity, when compared with that in normal gravity.

Recently, Takahashi et al. [21] investigated the extinction limits of spreading flames over wires both in normal gravity (1 g) and microgravity (μ g). Takahashi et al. [22] studied on unsteady molten insulation volume change during flame spreading over wire insulation in microgravity. Osorio et al. [23] studied the limiting oxygen index and limiting oxygen concentration of ethylene-tetrafluoro-ethylene (ETFE) insulated wires subject to an external radiant flux in both 1 g and μ g. Hu et al. [24] investigated flame spread rate over wire at different inclination angles with a high thermal conductivity metal inner core. Fujita [25] reviewed fire safety standards for flammability evaluation of solid material intended for use in a spacecraft habitat.

In 2006, we proposed a satellite project to investigate the pre-ignition characteristics of wire insulation by overload in microgravity, soot emission during the ignition stage, and the smoke distribution of the wire insulation combustion on board SJ-10 satellite [26]. The objectives are to study the smoke emission characteristics of wire insulations and to provide scientific data for the development of fire detection and fire alarm technology in manned spacecraft [27, 28].

In this chapter, we reviewed the research work on wire insulations completed by the authors. We first presented the functional simulation methods, then introduced the experiments completed in microgravity by using the China recoverable satellites of SJ-8 and SJ-10.

2 Research on Fire Initiation in Microgravity by FS Method

The natural convection almost vanished at microgravity. The heat transfer of the electric components is quite different at microgravity from on the ground. The heat loss of the electric components decreased at microgravity, it might cause the overheating of the electric components and then result in fire. However, this is a gradually developing process. Generally, it takes several minutes, several hours even more. To create such long duration microgravity (10^{-5} g) on the ground is almost impossible.

A “function simulation” method has been introduced to create such an environment on the ground. The term “functional simulation” (FS) means an environment was created on the ground, under the created condition; the heat transfer process is similar to that in microgravity due to the temperature elevation in the wire conductor and insulation by the effects of overload. That is the process of heat transfer in microgravity is simulated in normal gravity. This will be explained more clearly and theoretically in what follows.

The fundamental differential equations governing the incompressible Newtonian fluid two-dimensional “undefined” natural convective heat transfer are:

$$\text{Continuity : } \frac{\partial u}{\partial x} + \frac{\partial v}{\partial y} = 0 \tag{1}$$

$$\text{Momentum : } u \frac{\partial u}{\partial x} + v \frac{\partial u}{\partial y} = \beta \vartheta g + \gamma \frac{\partial^2 u}{\partial y^2} \tag{2}$$

$$\text{Energy : } u \frac{\partial t}{\partial x} + v \frac{\partial t}{\partial y} = \alpha \frac{\partial^2 t}{\partial y^2} \tag{3}$$

where

- β Coefficient of volumetric expansion, defined as $\beta = -\frac{1}{\rho} \left(\frac{\partial \rho}{\partial T} \right)_p$
- g Gravitational acceleration
- ϑ $T - T_\infty$
- ν Kinematic viscosity
- α Thermal diffusivity, defined as $\alpha = \frac{\lambda}{\rho C_p}$, λ is thermal conductivity

Based on these basic equations, similarity coefficients can be obtained through similarity analysis. Then the FS condition can be defined by analysis of the similarity coefficients.

For two stable incompressible natural convection fluids, under the conditions that the geometry and boundary conditions are similar, if the ratio of inertial force to viscosity, and the ratio of buoyant force to viscosity are similar at any corresponding point, the corresponding velocity field will be similar.

From the above basic equations, the Grashof number, expressed as $Gr_L = \beta g \vartheta L^3 / \nu^2$, can be conducted by similarity analysis. The Grashof number is representative of the ratio of buoyant force to viscosity. One of the characteristics of the natural convection is that the motive speeds rely on the ratio of buoyancy to viscosity. Thus, the Reynolds number can be expressed as $Re_L = f(Gr_L)$, which means that the Reynolds number is not an independent similarity modulus any more. In other words, the velocity fields for two kinds of stable incompressible natural convection fluids are able to be similar if only the Grashof number is similar at any corresponding point. The Nusselt number ($Nu = \alpha_c l_0 / \lambda_f$) is a dimensionless coefficient describing the heat transfer process under given conditions. It is a standard number to distinguish the heat convection similarity. The Prandtl number ($Pr = \mu c_p / \lambda$) is a dimensionless number of fluid properties. It describes the inherent relationship of velocity distributions and temperature profiles determined by the fluid properties. The Prandtl number for gas far from the critical state is approximately independent of gas temperature and pressure.

Thus, if the corresponding Prandtl numbers and Grashof numbers can be made to have the same values, the corresponding Nusselt numbers will then be the same. Therefore, the FS condition can be determined to be such that the Grashof numbers of the natural convective heat transfer in the two fluids are the same.

In microgravity, the effects of gravity are greatly reduced. If the microgravity environment defines as ten-millionth of Earth's gravitational environment, the FS condition can be determined by the relationship of Grashof number between microgravity and normal gravity. It is,

$$Gr_{\mu g} = \frac{\beta(10^{-5}g)\vartheta L^3}{\nu^2} = 10^{-5}Gr_L \quad (4)$$

As we know that,

$$Gr_L = \frac{\beta g \vartheta L^3}{\nu^2} = \frac{\beta g \vartheta L^3 \rho^2}{\mu^2} \quad (5)$$

According to the state equation for ideal gas:

$$\rho = \frac{p}{RT} \quad (6)$$

Then based on above the Eqs. (4), (5) and (6), we can obtain

$$p_{\text{simu}} = \left(\frac{g_{\mu g}}{g} \right)^{1/2} p \quad (7)$$

If the pressure ($p_{\text{simu}} = \sqrt{10^{-5}} p = 3.16 \times 10^{-3} p = 320.34 \text{ Pa}$) in the functional simulation experiment is achieved, it is easily to get $Gr_{\text{simu}} = Gr_{\mu g}$. Thus the FS condition is that the pressure in the simulated environment should be set at 320 Pa.

This dimensionless criterion is a property of fluid itself, which describes the inherent relationship between velocity field and temperature field. In the present case the Prandtl number of air is almost a constant which does not vary with its temperature and pressure.

In summary, for the natural convective heat transfer provided the Grashof number equals everywhere, the Nusselt number will also be equal everywhere. That means the simulation of heat transfer is satisfied. So, one can define the criterion of function simulation under the condition keeping the Grashof number equal everywhere.

Based on the concept of FS, a series of experiments have been conducted. Figure 1 shows the systematic diagram of the experiment system. The photograph of experimental set-up is shown in Fig. 2.

Three groups of civil class wire and six groups of astronautic class wire with different insulating materials, thickness of insulation, effective cross-section and rated current have been used in these experiments. Five different levels of environment pressure (100,000, 10,000, 1,000, 100 and 10 Pa) and five different currents (5, 10, 20, 30 and 40 A) have also been used in the experiments. For each wire with certain insulating material, certain thickness of insulation, certain cross-section at different levels of pressure and different currents a set of experiment results can be obtained. A few experiment results will be shown in the present paper. The temperature is the steady equilibrium temperature on the surface of the bare wire. The cross-section of bare wire is 1 mm^2 . The rated current is 20 A. It can be seen from the results that the steady equilibrium temperature greatly increases with the decrease in environment pressure when the current is larger than 20 A. For example, the steady equilibrium temperature is $131 \text{ }^\circ\text{C}$ when the environment pressure is 100,000 Pa and the current is

Fig. 1 Schematic diagram of experiment system

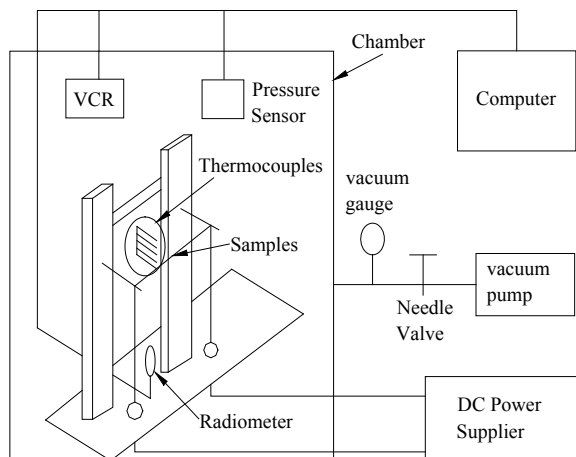


Fig. 2 Photograph of experiment set-up



30 A. However, the steady equilibrium temperature is 305 °C when the environment pressure is 100 Pa and current is still 30 A.

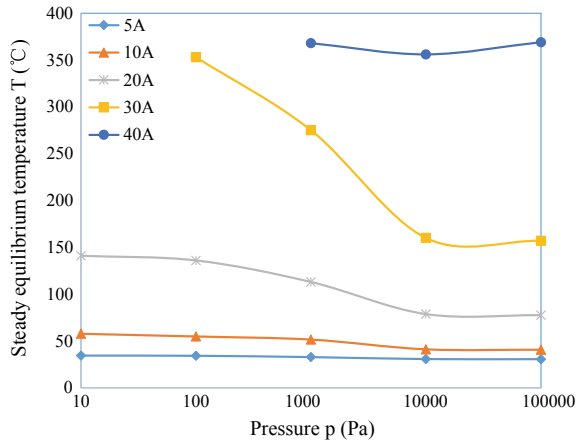
The experiment results of red copper wire insulated with polyvinyl chloride are shown in Fig. 3. The thickness of the insulation material is 0.6 mm. The cross-section of the bare wire is 0.75 mm². The rated current is 16 A. It can be seen from the results, that the steady equilibrium temperature is 157 °C when the environment pressure is 100,000 Pa and the current is 30 A. But the steady equilibrium temperature becomes 353 °C when the environment pressure is 100 Pa and current is still 30 A. This degree of overheat is not safe. It might result in the initiation of fire.

The experiment results obtained by the use of FS method proposed in present chapter indicate that at microgravity the natural convection almost vanished, the heat loss of the electric components decreased, it might cause the overheat of the electric components and then result in fire. The experiment results also verified clearly that the concept FS is a very effective method to simulate the heat transfer process of the electric components at microgravity.

3 The Low-Pressure Narrow Channel Method

A narrow channel method (NCM) was firstly proposed by Ivanov and Balashov [29] to study effects of buoyancy on flame spread over non-metal materials by the change of the value of the Grashof number, Gr , through adjusting the channel height.

Fig. 3 The steady equilibrium temperature of red copper bare wire with polyvinyl chloride



Zik et al. [30, 31] investigated the flame spread over thermally thin fuels, and observed the instability of fingering flames in the narrow channel. Wichman and Olson [32] and Olson et al. [33] studied the flame spread characteristics of thermally thin fuel by using different channel heights. It is found the observed flame was similar to that in the drop tower with a suitable channel height. Zhang et al. [34–36] further conducted experiments to study microgravity combustion phenomena by the narrow channel. Xiao et al. [37] also studied the effects of channel heights on flame spread rates and the flammability limit with the samples of the thermally thin fuels. The above studies have mainly focused on experimental investigations on the combustion characteristics of the thermally thin fuel using the narrow channel [30–37]. However, most non-metal materials used in the manned spacecraft are the thermally thick. The wire insulation used in this study is also a kind of thermally thick fuel [38]. The literatures of Wang et al. [38] and Xiao et al. [39] suggested that the channel height should be increased to investigate the microgravity combustion properties for the thermally thick fuels by the narrow channel. However if the channel height is increased, the Grashof number is also increased. The weakly buoyancy environment would be lost. Thus we should further study the narrow channel method to simulate the flammability of the thermally thick fuels in microgravity.

The FS method used in the last sections [13–15, 40, 41] is to simulate the natural convective heat transfer at microgravity by using a low pressure method (LPM). It means that the simulation is satisfied in heat transfer sense. The temperature variations of the wire insulation by using the LPM are similar to that at microgravity without combustion occurrence [16]. Once the ignition happens, the chemical reaction rate could be influenced by pressure, and resulted in the different combustion properties under LPM and microgravity. As for the NCM, on one hand, the smaller the channel height, the more similar results of the pre-ignition characteristics of materials to those at microgravity. On the other hand, if the height is too narrow (less than 10 mm), the wall cooling effect and the lack of oxygen transporting would significantly suppress

the ignition process. Besides, the conventional narrow channel could not be applied to study the thermally thick materials, like the wire insulation in this paper [38, 39].

To solve those problems, the LPNCM is combined the above two simulation methods to investigate fire initiation of thermally thick materials by firstly increasing the channel height and then reducing the ambient pressure. In this environment the Grashof number equals to that at microgravity. Based on the theory of similarity, the details are described as follows.

The Grashof number for a conventional NCM in 1 atm ambient pressure can be expressed as

$$Gr_{\delta} = (\beta_{\delta} g_0 \Delta T L_{\delta}^3 \rho_{\delta}^2) / \mu_{\delta}^2 \quad (8)$$

where β_{δ} is the coefficient of volumetric expansion, g_0 is the gravitational acceleration, ΔT is the temperature difference between the wire insulation and the air in the narrow channel, L_{δ} is the height of the narrow channel, ρ_{δ} is the air density and μ_{δ} is the air kinetic viscosity.

The Grashof number for LPNCM can be expressed as

$$Gr_{\delta p} = (\beta_{\delta p} g_0 \Delta T L_{\delta p}^3 \rho_{\delta p}^2) / \mu_{\delta p}^2 \quad (9)$$

The Grashof number at microgravity can be expressed as

$$Gr_{\mu g} = (\beta_{\mu g} g_{\mu g} \Delta T L_{\mu g}^3 \rho_{\mu g}^2) / \mu_{\mu g}^2 \quad (10)$$

Therefore the criterion of the LPNCM is

$$Gr_{\delta p} = Gr_{\delta} = Gr_{\mu g} \quad (11)$$

In order to minimize the influence of buoyancy, the Rayleigh number, Ra , should be less than a critical value Ra_{cr} [42]. Thus the criterion of both LPNCM and NCM for buoyancy to be negligible should be:

$$Gr_{\delta p} = Gr_{\delta} < Gr_{cr} = Ra_{cr} / Pr \quad (12)$$

where, Pr is the Prandtl number. It is almost a constant which does not vary with its temperature and pressure. So the critical value of the channel height of NCM for buoyancy to be negligible is:

$$L_{\delta, cr} = \sqrt[3]{\mu_{\delta}^2 Gr_{cr} / \beta_{\delta} g_0 \Delta T \rho_{\delta}^2} \quad (13)$$

Thus in NCM, the value of channel height L should be $L_q < L \leq L_{\delta, cr}$. Where, L_q is the quenching distance.

In addition, assuming that the ambient temperature and temperature variation in LPNCM are similar to those both in NCM and μg , β and μ could be treated as

the same value. In fact, the changing of environmental temperature in those cases only causes small changes of β and μ , which has been neglected. And this is one assumption of the LPNCM. Besides, substituting the ideal gas equation of state $\rho = p/(RT)$ to Eq. (11), this yields the criterion for the choice of the channel height of LPNCM:

$$L_{\delta p}/L_{\delta} = \sqrt[3]{p_{\delta}^2/p_{\delta p}^2} \quad (14)$$

According to Eq. (14), in LPNCM if the ambient pressure is reduced to $p_{\delta p}$, the channel height should be increased to $L_{\delta p}$. From Eq. (12), the critical value of the channel height of LPNCM for buoyancy to be negligible is:

$$L_{\delta p,cr} = \sqrt[3]{\mu_{\delta p}^2 Gr_{cr}/\beta_{\delta p} g_0 \Delta T \rho_{\delta p}^2} \quad (15)$$

According to the FS method in last section combined with LPM, the critical value of pressure used in LPNCM is obtained as

$$p_{\delta p,cr}/p_{\mu g} = \sqrt{g_{\mu g}/g_0} \quad (16)$$

It is the minimum pressure used in LPNCM. So the pressure range for LPNCM is

$$p_{\delta p,cr} \leq p_{\delta p} \leq p_{\delta} \quad (17)$$

Usually, the value of the ambient pressure is 1 atm for either NCM or μg . The residual gravitational acceleration at microgravity is $10^{-5}g_0$. Thus the critical value of pressure used in LPNCM can be obtained. Substituting this critical pressure into Eq. (15), the critical value of the channel height should be the maximum value used in LPNCM. Meanwhile, substituting the value of p_{δ} into Eq. (15), this yields $L_{\delta p,cr} = L_{\delta,cr}$. Therefore the range of channel height in LPNCM is

$$L_{\delta,cr} \leq L_{\delta p} \leq L_{\delta p,cr} \quad (18)$$

From Eq. (11), for two specific conditions in the LPNCM, the value of $L_{\delta p}$ should be satisfied the following relationship.

$$L_{\delta p1}/L_{\delta p2} = \sqrt[3]{p_{\delta p2}^2/p_{\delta p1}^2} \quad (19)$$

Thus, in the LPNCM, the pressure could be decreased to increase the narrow channel height and L could be chosen according to Eq. (19), which is the principle of the LPNCM. And the specific value of L in the LPNCM should be decided by the detailed experimental conditions, considering the size of thermal thick fuel and the simulated level of gravity. In the following, the effectiveness of LPNCM would be verified by the experimental results.

According to the principle of the LPNCM, a narrow channel setup operated at low-pressure environment (less than 1 atm) has been set up to achieve the weakly buoyancy environment. Figure 4 is the schematics of experimental setup for the tests here. It is consisted with a cabin, a narrow channel system, a vacuum system, a sample setup, an electrical power supply and a measurement system. The experimental cabin is a stainless steel cylinder with a height of 500 mm and an outer diameter of 400 mm. The sample of wire, the narrow channel setup, thermocouples, and the CCD camera were installed inside the cabin. While a vacuum pump, vacuum gages, a constant current supply and data collection system were arranged outside the cabin.

The narrow channel setup is consisted with two pieces of horizontal quartz plate with a thickness of 4 mm, length of 290 mm and width of 140 mm. The channel height H can be adjusted from 10 to 120 mm. The cabin inner ambient pressure p can be adjusted by the vacuum pump. The experiments were conducted in the quiescent environment at fixed pressure p . The temperature histories of the wire insulation and its surrounding environmental temperature variations were measured respectively by K-type thermocouples, all with a diameter of thermocouple wire of 0.2 mm and a sheath diameter of 1 mm. The thermocouple touched the wire insulation surface closely with the hot junction. Five measurement points were arranged around the wire. Three thermocouples were touched the wire insulation with a horizontal distance of 20 mm. Two thermocouples were arranged to measure the surrounding ambient temperature. There are located on the upper and lower sides of a thermocouple touched in the insulation with a vertical distance of 5 mm. This arrangement of measurements can obtain the temperature history of the wire insulation and the representative temperature raising results of its surrounding area. In experiments, polyethylene insulated nickel–chrome wire specimens were used. Each wire is 0.5 mm in inner diameter. The thickness of wire insulation is 0.4 mm. The effective sample length is 70 mm. The rated current for this wire is 1 A. The oxygen concentration inside the cabin was 21% (N_2 diluent) at different pressures.

Fig. 4 Schematics of experimental setup by LPNCM

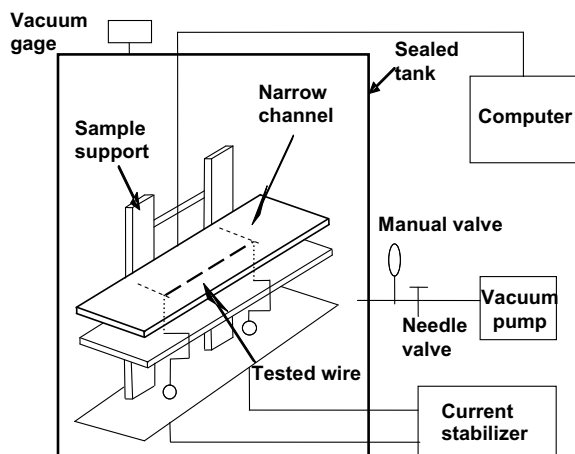


Table 2 Four equivalent conditions of LPNCM

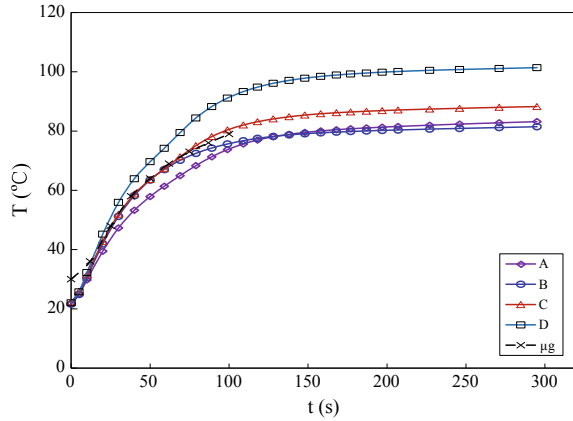
| Condition | Narrow channel height, mm | Pressure | Current, A |
|-----------|---------------------------|----------|------------|
| A | 10 | 1 atm | 2, 6 |
| B | 13.6 | 63 kPa | 2, 6 |
| C | 21.4 | 32 kPa | 2, 6 |
| D | 46.4 | 10 kPa | 2, 6 |

Using the parameters provided in Refs. [34, 35, 39], the critical channel height in NCM can be calculated by Eq. (6) with a result of 10 mm at 1 atm. Thus the experimental conditions in LPNCM can be determined by Eq. (19). The results are listed in Table 2, where typical values of pressure were used based on our previous study [40]. It is seen from Table 2, the pressure and the channel height can satisfy the requirement of Eq. (19). In the experiments, two typical values of current of 2 A and 6 A were used to investigate the effect of current on the fire initiation characteristics of wire insulation. By moderate overload current of 2 A, the temperature variations of the wire insulation were obtained without the wire damaged. While by current overload of 6 A, the wire was breakdown with smoke released from the wire insulation.

3.1 Temperature Variation of Wire Insulation with 2A

Figure 5 shows the variations of the surface temperature of wire insulation at different experimental conditions as shown in Table 2 conducted by the LPNCM with 2 A current. According to the measurement arrangement, there are three thermocouples used to monitor the surface temperature histories of the insulation. It is the temperatures of T_3 , T_4 and T_5 . The results, shown in Fig. 5, are the arithmetic average of the three temperatures. It is seen from Fig. 5 that the temperature increased rapidly after the power on, about 100 s later the temperature increasing rate slowed down and gradually attained a quasi-steady equilibrium state between the heat produced by the wire and the heat loss from the insulation to the environment. The temperature variation trends are the same as our previous experimental results [16]. It is also seen from Fig. 5 that the temperature rising rates for cases A, B and C were almost the same, while it is different for case D. The temperature rising rate for case D is maximum among them. And the reason for the differences would be discussed later. Furthermore, when compared with the temperature histories of microgravity [5], it can be found that the temperature rising rates for cases B and C are agreement very well with the results conducted in microgravity. Though the initial temperature of wire insulation is 30 °C, 10 °C higher than that in LPNCM, and the wire heating power is 1.27 W [5], a little bit smaller than 1.3 W in LPNCM, the temperature versus time for cases A, B and C, are quite similar with that in microgravity. It proves the validation of LPNCM in simulation of temperature variation characteristics of wire insulation in microgravity.

Fig. 5 The temperature histories by LPNCM with moderate overload current of 2 A (the temperature histories of “ μg ” are microgravity results from Greenberg et al. [5])



Moreover, we can read the temperature rising time t_p , which is defined as the duration from power on to reach the steady equilibrium temperature, from Fig. 5. Figure 6 shows the variations of t_p under different experimental conditions by LPNCM. As comparison, the results conducted by NCM are also presented there. It is seen from Fig. 6 that the value of t_p decreases quickly with the increase of channel height by NCM, while it keeps similar value in LPNCM for cases A, B and C. In NCM, the effect of buoyancy increases obviously with the increase of the channel height at 1 atm, which leads to the increase of the heat transfer in convection and better cooling conditions for the wire insulation so that t_p of the wire insulation decreases gradually. In LPNCM, the value of t_p for cases A, B and C are almost the same within error limits, because the effect of buoyant convection is still suppressed effectively in the larger channel height with lower pressure environment so that the cooling conditions are similar in those cases. Then, the heat produced by the overloaded current cannot move away through the insulation surface quickly, and thus the value of t_p is similar for those cases. As for comparison, the microgravity result of Greenberg et al. [5] is also presented in Fig. 6. It is seen that the present results of case A, B and C are quite close to that in μg . This again proves that the validation of LPNCM. The parameters for case A, B and C, calculated by Eqs. (10)–(12), satisfies the similarity criterion of LPNCM. While for case D, the value of t_p is increasing to a pretty large value not satisfying the method, which would be discussed later.

We can also obtain the steady equilibrium temperature (T_p) from the temperature histories recorded by different thermocouples with the conditions described in Table 2. Figure 7 shows the steady equilibrium temperature under different experimental conditions. The thermocouples No. 3, 4 and 5 were used to monitor the insulation surface temperature. Point 3 was located at the upper side, while the test point 4 and 5 were located at the down side and with the same vertical height. Thus, the data of T_{4p} shown in Fig. 5 are the average temperature records of T_4 and T_5 . In Fig. 7, the solid lines were present results by LPNCM, while the dotted lines were the previous results by NCM from Wang et al. [38]. According to Fig. 7, it is seen that

Fig. 6 The contrast of t_p obtained by both LPNCM and NCM with current of 2 A (the t_p of “ μg ” is the microgravity result from Greenberg et al. [5])

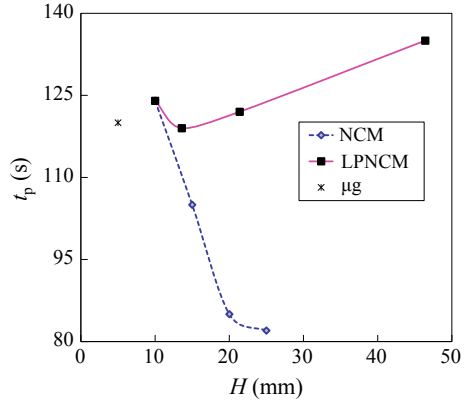
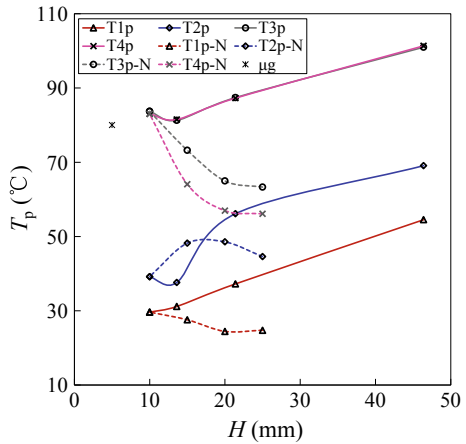


Fig. 7 The steady equilibrium temperature under different experimental conditions of 2 A. The solid lines were present results by LPNCM, meanwhile the dotted lines were the previous results by NCM (the T_p of “ μg ” is the microgravity result from Greenberg et al. [5])



the results of the insulation surface temperature of T_{3p} and T_{4p} have the same values. This indicates that the temperature of insulation has the same value by LPNCM. For cases A, B and C the temperature differences of T_p are not large. While for case D, T_p increases obviously, and it is far larger than the others. The explanation is as follows. For case D, the pressure was very low (10 kPa), the natural convection was greatly inhibited, and the heat loss of the insulation was decreased, which resulted in the increase of the steady equilibrium temperature. It proves that the effect of lower pressure has overpassed the effect of narrow channel. Thus, the LPNCM is effective to build a weakly buoyant environment and limit the heat transfer of natural convection. However, the environmental pressure should be decreased within a proper range to achieve the similar variation tendency of temperature in above conditions. For example, to obtain similar temperature histories of T_3 of condition A, the value of pressure is suggested to be not less than 32 kPa.

The reason of the limitation has been provided as follows:

According to the ideal gas equation of state, the mass of air in the narrow channel is $m = pV/(RT)$. Based on Eq. (19), we could obtain the following equation:

$$m_{\delta p1}/m_{\delta p2} = \sqrt[3]{p_{\delta p1}/p_{\delta p2}} \quad (20)$$

Thus, the total amount of air in the narrow channel decreases with the decrease of pressure. Then if the pressure is too lower (10 kPa in case D), the total amount of air in the narrow channel is decreased too much, which causes the temperature of points near the wire insulation to rise more quickly than that in higher pressure with smaller narrow channel. Then the β and μ of the environment would change greatly so that the LPNCM is inapplicable. That's the reason for the case D not satisfying the method.

It is also seen from Fig. 7 that T_p is decreased with the increase of the channel height in all cases of NCM (after H is greater than 15 mm). This indicates that NCM can be used to simulate microgravity condition only as the channel height is smaller than a specific value (15 mm in this paper). With the increase of the channel height, the buoyancy induced convection is enhanced in NCM. While, for cases A, B and C of LPNCM, T_p is not decreased with the increase of the channel height. Moreover, either T_p of T_{3p} or T_p of T_{4p} in LPNCM is close to that in μg . Thus, LPNCM could effectively suppress the buoyancy induced convection, which could be used to simulate the microgravity environment.

Finally, according to the T_p temperature difference shown in Fig. 7, the uniformity of temperature distribution near the wire insulation could be judged. As for the pair of symmetric points of 3 and 4, the temperature T_p variation curve of T_3 is nearly the same as that of T_4 in the LPNCM, which means that the temperature distribution is uniform in the vertical direction. However, as shown in Fig. 7, the T_p temperature difference in the NCM conditions increases with the increase of the channel height, which means the non-uniformity of temperature distribution in the vertical direction. Thus, when compared with the NCM, the LPNCM improves the uniformity of temperature distribution near the wire insulation.

In summary, the criterion of Eqs. (10)–(12) for LPNCM is experimental proved to be useful in determining the experimental condition. The narrow channel height can be increased from 10 to 21.4 mm by decreasing the pressure from 1 atm to 32 kPa with the LPNCM, which is effective to simulate the temperature variations in microgravity.

3.2 Smoke Emission with 6 A in LPNCM Conditions

As the value of current increases to 6 A, wire insulation will be damaged quickly. A large amount of smoke is emitted without flame. Thus the wire insulation is in the smoke producing stage of fire initiation. The process of smoke producing and moving has been recorded by a CCD camera. The four conditions of LPNCM have been

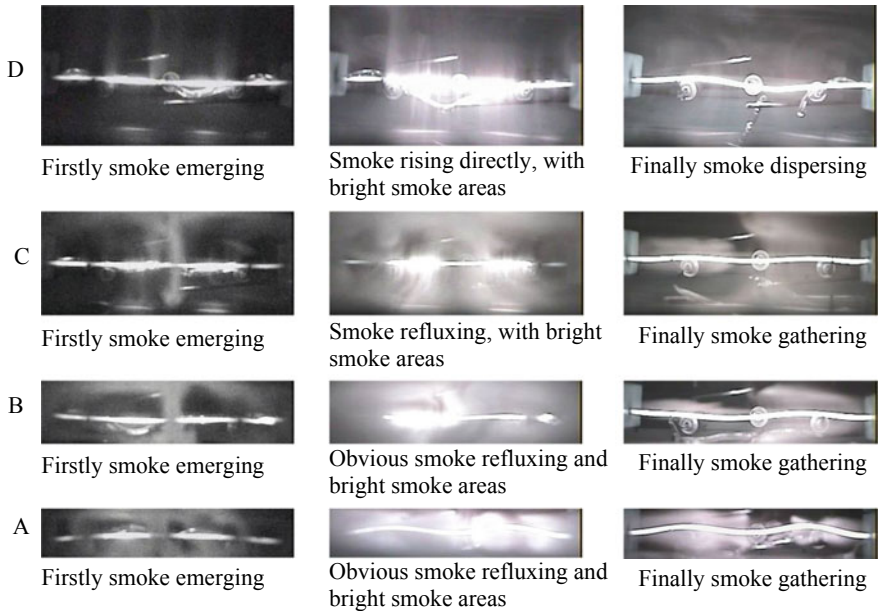


Fig. 8 The smoke emission characteristics by LPNCM with current of 6 A

conducted and repeated three times, with good repeatability. The smoke emission characteristics from wire insulation have been shown in Fig. 8. Three kind of typical stages were chosen and shown in Fig. 8 to describe the smoke emission characteristics of wire insulation as follows. (1) The beginning stage: the smoke begins to produce and its distribution state could be obtained at the early stage. (2) The highlight stage: after a large amount of smoke produced, smoke moves toward outside, with track of circumfluence, due to the confinement by the narrow channel [38]. Meanwhile, there are bright smoke areas along the wire insulation. A highlight smoke distribution area can be observed as strong smoke movement. (3) The evanescent stage: at the end of smoke movement, the accumulated smoke near the wire insulation would evanesce and the distribution state of the left smoke could be observed.

According to Fig. 8, we can analyze the similarity of smoke moving characteristics in four conditions of LPNCM, which has been listed in Table 3. (1) The beginning stage: case A, B and C have the similar smoke moving characteristics—the smoke is emitted from the center area of the wire insulation and then symmetrically moves toward left and right. The shape of the smoke is like a mushroom. However for case D, it has great difference in the smoke moving characteristics. The smoke moves upward directly. There is no clear smoke area under the wire insulation and its distribution of smoke is like an upended curtain in shape. (2) The highlight stage: case A and B have the similar smoke moving characteristics. A group of bright smoke is accumulated near the wire insulation, strong circumfluence movement could be found due to the confinement of the narrow channel, which is similar with that in

Table 3 The contrast of smoke moving characteristics in LPNCM at 6 A

| Condition/stage | The beginning stage | The highlight stage | The evanescing stage |
|---|---|---|--|
| A (10 mm, 1 atm) B (13.6 mm, 63 kPa) | The smoke is discharged from the center area of the wire insulation and then symmetrically moves toward left and right; the distribution of smoke is like a mushroom in shape | A group of bright smoke is gathered nearby the wire insulation, fierce circumfluence movement could be found due to the confine of narrow channel | The left smoke has the similar moving characteristics, gathering around the wire insulation and moving along it slowly |
| C (21.4 mm, 32 kPa) | | The concentration of smoke begins to decrease, with some circumfluence movement, and a smaller group of bright smoke gathers around the wire insulation | |
| D (46.4 mm, 10 kPa) | The smoke moves upward directly and its distribution of smoke is like an upended curtain in shape | The concentration of smoke becomes the least and a large amount of smoke move upward, with less smoke circumfluence movement | The smoke evanesces directly and there is no smoke gather around the wire insulation |

microgravity [5]. In the condition of case C, the concentration of smoke begins to decrease, with some circumfluence movement, and a smaller group of bright smoke accumulated around the wire insulation. However, for case D, the concentration of smoke becomes small and a large amount of smoke move upward, with less smoke circumfluence movement, which shows small assembling effect of smoke around the wire insulation as comparison with the other conditions. (3) The evanescing stage: At the end of smoke moving, in case A, case B and case C, the residual smoke has the similar moving characteristics, accumulating around the wire insulation and moving along it slowly. Greenberg et al. [5] and Fujita et al. [19] have investigated the movement of smoke from the wire insulation in microgravity after ignition. Results show that smoke resides near the wire insulation for a relatively long period, and then propagates along the wire gradually in microgravity. While smoke would move upward the wire insulation as a result of buoyancy induced flow in normal gravity. Thus, the smoke uniformly moving along the wire in LPNCM has effectively simulated the key movement characteristic of smoke in microgravity. However, in case D, the smoke evanesces directly and there is no smoke accumulated around the wire insulation.

In summary, by the analysis of smoke moving characteristics, case D has great differences with the other conditions, which could not be regarded as an equivalent condition. The others are observed similar smoke moving characteristics at the typical stages. According to our previous results [38], in normal gravity and 1 atm ambient pressure of NCM, if the channel height is greater than 15 mm, it cannot be used to simulate the smoke moving characteristics at microgravity. Besides, results in this paper showed if the pressure reduced to 32 kPa and the narrow channel increased to 21.4 mm, LPNCM can still be used to simulate the phenomena at microgravity, for example it could obtain similar smoke moving characteristics at microgravity.

4 Study on Prefire Phenomena at Microgravity by SJ-8

4.1 *Experimental Facility and Process*

The experimental setup was designed for microgravity experiments at the China recoverable satellite SJ-8, which offers long microgravity experimental duration and 10^{-4} g microgravity quality and requires experiments that are operator-independent, compact, and constructed to withstand vibrations, large rate of deceleration and meet stringent safety standards. The setup was a stainless-steel cylindrical vessel with an outer diameter of 320 mm, a wall thickness of 2 mm and depth of 450 mm. Figure 9 is a photo of the flight experimental package. It was mainly a test section with a constant current supply to provide overloaded current, a thermocouple temperature measurement system, a radiometer system and a controls system. They were fitted on three levels.

The test sample wires, thermocouples and radiometers were mounted on the first level. The polytetrafluoroethylene-insulated silver-gilt copper wire was used as the test sample. It is an astronautic grade wire cable with black colour. The cable conductor is consisted of 19 pcs single wire. Each wire is 0.12 mm in diameter. The criterion section area of the cable is 0.2 mm^2 . The thickness of cable insulation is 0.1 mm. The rated current for this cable is 2 A. In order to investigate the effects of the overload current on the fire initiation of the wire insulation, two cables were used in the experiments. Each cable was fixed to the sampling holder with a length of approximately 100 mm, and then it was coiled closely around an insulated flame retardant pole. The pole is a silicone rod with diameter of 5 mm. The typical properties of the silicone holder are as follows: thermal conductivity of 0.9 W/m K, surface resistivity of $1.38 \times 10^{14} \Omega$, dielectric constant of 2.5 MHz. In the experiments, the temperature histories of the uncoiled wire and the coiled part were measured respectively by K-type thermocouples, all with a sheath diameter of 0.5 mm. For the coiled part temperature measurement, the thermocouple was embedded inside the surface between two coiled wires. For the single wire temperature measurement, the thermocouple touched the wire insulation surface closely with the hot junction. The radiometer was used to measure the radiation emitted from the coiled wire insu-

lations. It is an infrared radiometer with film thermopile. The reason for using the coiled wires for radiation measurement is to increase the detectable area to satisfy the radiometer requirements. Furthermore, we can use one wire to investigate the effects of wire bundles on fire initiation.

The second level of the experimental apparatus was the controls level. It consisted of the central control module, the information module, the relay, the A–D data collection module, and the DC electrical supply, where the DC electricity was supplied by the satellite. All the temperature transducers, radiometers, current transducer and pressure transducer were connected to the AD data acquisition card. All these data were packed up and communicated with the ground control centre.

The constant current supply, providing the overloaded current for the test wire cable, was fitted on the third level.

The pressure in the experimental module at the satellite was lower than the ground ambient pressure. It was about 59 kPa. Thus the low-pressure experiments at normal gravity were conducted to comparing with the microgravity results.

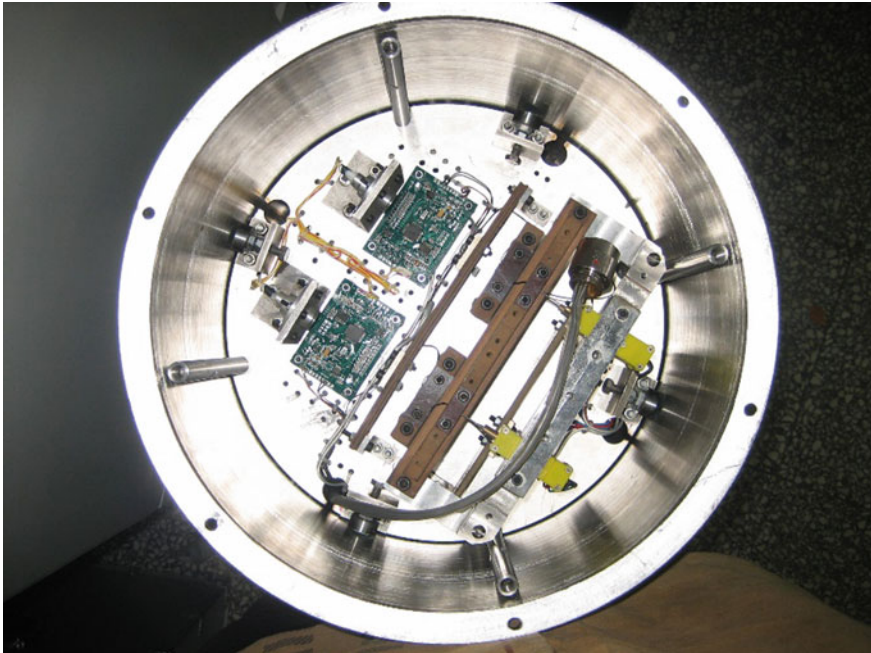


Fig. 9 Photo of the flight experimental package

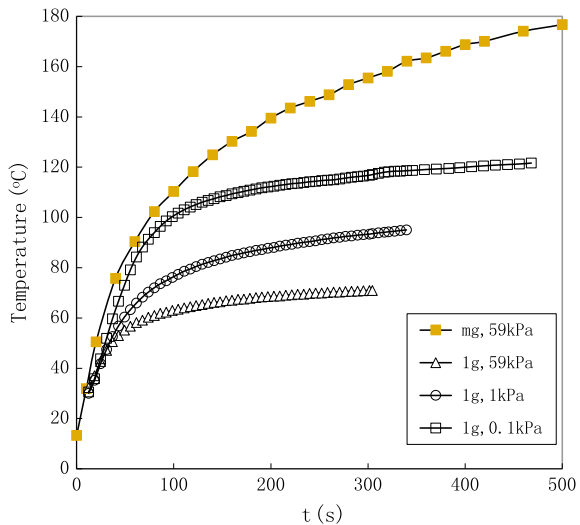
4.2 Temperature Histories

The temperature histories of the coiled wire insulations at microgravity with overloaded current of 10 A are shown in Fig. 10. It is seen from Fig. 10 that the temperature increased rapidly after the current inputted, then the temperature increasing rate slowed down and gradually attained a quasi-steady state between the heat produced by the overload and the heat loss to the environment.

The results indicated that the buoyant convection decreased and almost vanished, the heat loss decreased. Thus, the heat produced by the overloaded current cannot move away through the insulation surface immediately, and thus the insulation temperature is gradually increasing. The results also indicated that the heat loss of the electric components decreased at microgravity, it might cause the overheating of the electric components and then results in fire. This is a gradually developing process. It takes several minutes, several hours even more. To create such long duration microgravity on the ground is almost impossible. However space flight experiments at the real microgravity environments are very expensive. It is unsuitable for lots of material tests. Therefore a “function simulation” method is introduced here to create an environment on the ground where the heat transfer of electric wire, cable and components are similar with that at microgravity. So that plenty of experiments can be completed to satisfy requirements of fire safety at microgravity. The suggested experimental method is functionally satisfied in heat transfer sense. The principle and conditions for function simulation are discussed in more detailed in the following.

For flame spread at different pressure environments, the impact of radiative losses can be estimated by the radiative time scale t_{rad} . It can be expressed as $t_{rad} = T_f \rho c_p / (4\sigma a_p (T_f^4 - T_\infty^4)) \sim \rho / a_p$, where optical thin model is used for

Fig. 10 Temperature histories of the coiled wire insulations at microgravity and normal gravity with current of 10.2 A



the radiative loss from a volume of gas at the flame temperature T_f . Since the Planck mean absorption coefficient of the gas has $a_p \sim P^1$, assuming an ideal gas, we have $t_{rad} \sim P^0$. Thus, the radiative time scale is similar at all pressures. Therefore, in the following analysis to determine the function simulation conditions, the radiative heat transfer is neglected.

For the incompressible Newtonian fluid two-dimensional “undefined” natural convective heat transfer, the Nusselt number can be defined as the ratio of convection heat transfer to fluid conduction heat transfer under the same conditions. It is a dimensionless criterion measuring the convective heat transfer coefficient under certain defined circumstances. It is also a similarity criterion distinguishing whether the convective heat transfer is similar. The Prandtl number is a dimensionless parameter of a convective system that characterizes the regime of convection. This dimensionless criterion is a property of fluid itself, which describes the inherent relationship between velocity field and temperature field. In the present case the Prandtl number of air is almost a constant which does not vary with its temperature and pressure. The Grashof number is a dimensionless number in fluid dynamics which approximates the ratio of the buoyancy to viscous force acting on a fluid. The characteristic of natural convection is that the fluid velocity depends only on the ratio of buoyancy to viscous force. Meanwhile, for natural convection the Reynolds number is no longer an independent similarity criterion. Only the Grashof number equals everywhere the velocity field will be similar. Thus, for the natural convective heat transfer provided the Grashof number equals everywhere, the Nusselt number will also be equal everywhere. That means the simulation of heat transfer is satisfied. So, one can define the criterion of “function simulation” under the condition keeping the Grashof number equal everywhere.

We know the Grashof number is $Gr = (\Delta\rho/\rho)gL^3/v^2 \sim P\Delta\rho gL^3/\mu^2$. If the reduced gravity of $10^{-4}g$ is utilized and density variation induced by temperature is assumed to be independent of pressure, the relationship of reduced pressure for function simulation P_s and the pressure at microgravity P_{mg} can be expressed as: $P_s = 10^{-4}P_{mg}$. Thus by using reduced ambient pressure in normal gravity can realize the identical Grashof number at microgravity.

Figure 10 shows experimental results under reduced pressures of 59, 1 and 0.1 kPa. It is seen from Fig. 10 that the temperature varying tendencies are all the same under function simulations and microgravity environment. The temperature increased rapidly after the current inputted, and then the temperature change tendency was slowed down to attain their maximum value, after that the temperature remained almost unchangeable. We define these maximum values of temperature as the steady equilibrium temperature of the wire insulations under the experimental conditions. It is seen from Fig. 10, the steady equilibrium temperature greatly increased with the decrease of the environment pressures in normal gravity. In the experiments, the steady equilibrium temperature was 70 °C at pressure of 59 kPa, while it was 120 °C at pressure of 0.1 kPa. This is because that the decrease of the environment pressure leads to the decrease of the buoyancy convection, and thus the heat loss of the wire insulation decreased. Therefore, the temperature of the wire insulations increased with the decrease of the pressures.

From the discussions of functional simulation, to achieve the presented microgravity experimental condition, the reduced pressure should be around 5.9 Pa. This is not achieved in Fig. 4's reduced pressures experiments completed in normal gravity. Thus the microgravity data do not fit to any of the reduced pressure data.

The steady equilibrium temperature T_s at quasi-steady state can simply estimate from the balance of heat fluxes between conduction, convection and radiation. The results can be expressed as: $T_s \sim \alpha^{-1} \sim Nu^{-1}$. Where α is the heat transfer coefficient. From the classical heat transfer textbook, we know the Nussle number and Grashof number have relation of $Nu = f(Gr^n)$. Thus the steady equilibrium temperature can be expressed as: $T_s \sim Gr^{-n}$.

Table 4 shows the experimental temperature and rough estimated results by the exponent (n) relation of $T_s \sim Gr^{-n}$. Where $n = 0.12$.

It is seen from Table 4, with $n = 0.12$, the estimated results by using of the relation $Nu = f(Gr^n)$ agreed very well with the experimental results. Actually, the exponent (n) in relation $Nu = f(Gr^n)$ is about 0.12 can be found in many literatures on heat transfer from a cylinder [43]. Using this value, predicting the microgravity data is possible by extrapolation to the 10^{-4} g in the g term in Grashof number. In Table 4 the pressure of 5.9 Pa is the functional simulation condition of the microgravity environment of 10^{-4} g. The predicted steady equilibrium is slightly larger than the microgravity experimental data. The reason is that at microgravity experiments the steady equilibrium has not achieved yet. Thus it is reasonable to declare that the predicted reduced pressure value is agreed with the microgravity experimental results. Thus the heat transfer of buoyancy convection explains the observed trend very well.

The temperature histories of a single wire and the coiled wire measured by thermocouples in the microgravity environment. The cable wire coiled closely around the insulated flame retardant pole, which is used to simulate the parallel arrangements of cables required by ASME cable standard. It was observed that the insulation temperature change tendency is the same for the single wire and coiled wire, but the temperature increasing rate and the final reached maximum temperature during the experiments are quite different. The insulation temperature behaves firstly increasing quickly and then the temperature increasing rate slow-down, where the temperature increasing rate can be inferred from the results. For the single wire, the insulation temperature increased from 13.2 to 43.5 °C in the time duration of 140 s, and thus the

Table 4 Experimental and estimated results of steady equilibrium temperature

| Conditions | Experimental results, °C | $T_s \sim Gr^{-n}$, °C |
|--------------------------|--------------------------|-------------------------|
| P = 59 kPa | 70 | 61.22852 |
| P = 1 kPa | 95 | 99.87482 |
| P = 0.1 kPa | 125 | 131.6607 |
| P = 5.9 Pa | | 184.9072 |
| Microgravity 10^{-4} g | 176 | |

temperature increasing rate is $0.217\text{ }^{\circ}\text{C/s}$. While in the same time duration, the insulation temperature increased from 13.2 to $124.9\text{ }^{\circ}\text{C}$ for the coiled wire, and results in a temperature increase rate of $0.798\text{ }^{\circ}\text{C/s}$. In the whole experimental duration, the final insulation temperature of the coiled wire was $234\text{ }^{\circ}\text{C}$, while the final insulation temperature for the single wire was $88\text{ }^{\circ}\text{C}$. It infers that the heat loss decreased quickly in the wire coiled case than that in the single wire case at microgravity. Therefore, from our experimental results, it is concluded that it is easier to cause the over heat of the electric components and then results in fire for the wire bundle situation in the microgravity environment.

4.3 Effects of Overloaded Currents

In the space experiments, two kinds of overloaded currents were used to investigate the effects of overloaded currents on the temperature profiles of the wire insulations. The currents varied from 9.9 to 10.2 A . The current difference is 0.3 A . The imperceptible difference in manufacture may lead to a small difference in resistance of the wire or cable. These differences may cause disaster under overloaded conditions, and thus the purpose of using a small current difference in the experiment was to investigate the trivial difference in overloaded current may cause what happen to the wire insulation. The results conducted in microgravity condition show that the temperature histories of the single wires under overloaded currents of both 9.9 and 10.2 A were almost the same. It means that the difference of 0.3 A of the overloaded currents cannot bring significant difference for the single wire in the microgravity condition. Whereas for the coiled wire the difference of overloaded current, even as small as 0.3 A , resulted in the observed difference of the temperature profiles. It is seen from the results, the insulation temperature variation can be divided into two stages. In the first stage, the temperature increased quickly, and then the temperature variation changed to the second stage, where the temperature increase rate slowed down. In the second stage, the insulation temperature increased gradually. It is observed that the effects of currents were mainly in the first stage. The insulation temperature increasing rate increased with the increase of the overloaded currents, and thus the attained maximum temperature in the first stage increased with the increasing the overloaded current. In the second stage, however the temperature increasing rate was almost the same for the different currents used in the experiments. The final insulation temperature increased with increasing the overloaded currents.

4.4 The Radiation Characteristics

Radiation is one of the most important factors involved in fire initiation of wire insulation caused by overload. The radiation signal can be used for fire monitor. The radiation energy emitted from the insulation was measured by an infrared radiometer.

The infrared lens is a germanium crystal. It can detect the low-temperature radiation energy. The radiometer is specially designed for the experiments. The temperature range is from -10 to 500 °C with 1.5% accuracy. It constructed to withstand vibrations and satisfied other stringent requirements for space experiments. Due to the radiation energy being not intuitive, the output of the radiometer was transferred to the temperature reading. Hereafter we denoted it as radiation temperature. The radiation temperature of the radiometer was calibrated by the blackbody calibration system.

It is seen from the results that the radiation temperature increased with the increasing the overloaded currents. During the experiments, the radiation temperature increased continually. It implies that the steady equilibrium between the heat produced by the overload and the heat loss to the environment is never achieved at microgravity. It is in reason to infer that the overheating of the electric components might finally result in fire if the current never be switched off. The change tendency of the radiation temperature was similar to that of the thermocouple temperature readings. However the thermocouple temperature reading is greater than the radiation temperature in approximately 50 °C. The results demonstrated that the temperature inside the coiled wire was greater than the radiation temperature emitted by the insulation surfaces.

The experimental hardware has been developed to perform the experiments of fire initiation of wire insulation caused by overload on board the China recoverable satellite. The present results show that the temperature of the wire insulation increased continually in the microgravity environment, while in normal-gravity, the temperature might finally attain quasi-steady equilibrium even in low-pressure environment. The steady equilibrium temperature increased with the decrease of the pressure due to the suppression of the buoyancy convection in low-pressure environment. The results imply that the low-pressure environments can be used to simulate the microgravity environments for the study of the fire precursor of wire insulation. The simulation is satisfied in heat transfer sense by selecting different pressure to simulate different gravity level. Nevertheless the results indicate that the microgravity experiments cannot be replaced absolutely by the simulation method in normal-gravity. The effects of wire bundle were investigated at microgravity. The results showed that the insulation temperature of the coiled wire was much greater than that of single wire. Therefore, it is easier to cause the overheating of the electric components and then results in fire for the wire bundle situation in the microgravity environment. The effects of overloaded currents on the insulation temperature and radiation characteristics of the coiled wire were presented. The results showed that temperature increased with the increasing current. For coiled wire the radiation temperature was less than the insulation temperature obtained by thermocouples. The results demonstrated that the temperature inside the coiled wire was greater than the radiation temperature emitted by the insulation surfaces. The experiment results indicate that at microgravity the natural convection almost vanished, the heat loss of the electric components decreased, it might cause overheating of the electric components and then results in fire. The results show that the fire risks of wire overload in the microgravity environment are much more serious than that in normal-gravity.

5 Wire Insulations Experiments in Microgravity by SJ-10

5.1 Setup of Experiment on SJ-10

The long-term overloaded wire insulation combustion (LOWIC) space experiment was performed in one payload of the 24th recoverable satellite of China, the SJ-10 satellite [26, 44, 45], carried by the CZ-2D carrier rocket at 1:38'04" am, April 6, 2016. The payload was sent into the 250 km earth orbit, offering high-quality (better than 10^{-3} g, @ ≤ 0.1 Hz) microgravity for long experimental duration [46].

Figure 11a shows the setup. It was mainly a test section with a constant current supply to provide overloaded current, a thermocouple temperature measurement system, a soot volume fraction measurement system and a controls system. We applied the laser extinction method to analyze the smoke emission in high-concentration zone. A laser generator (wavelength: 635 nm, installed with a spatial filter), two mirrors, two convex lens, a beam splitter lens, and two 8-bit black and white CCD cameras (resolution: 1024×776 pixel, acquisition rate: 25 Hz, observing diameter: 78 mm) were fixed on an optical platform. The CCD camera 2 captured images directly, and the CCD camera 1 recorded tests through the light extinction path. We left a tiny angle between the direct optical path and the light extinction path. We installed a pressure sensor (Honeywell ASDX030P-AAA5, range: 0–1.5 atm, accuracy: 1 kPa), an oxygen sensor (range: 0–100%, accuracy: $\pm 0.01\%$), and seven K-type nickel chromium-nickel silicon thermocouples (diameter: 0.2 mm, range: 0–900 °C, accuracy: $\pm 0.4\%$) to record parameters. The 28 V power was supplied by the satellite and the current was changed by modifying the duty cycle of the wire [47].

Figure 11b shows the sample configuration of the LOWIC experiment. Seven insulated Cr20Ni80 wires (core diameter: 0.5 mm, total resistance: 0.356Ω) were held and fastened in a wire holder (three in a horizontal column and four in a vertical column). The effective length of cores was 70 mm, and the insulation length was 40 mm. The two columns were 16 mm apart from each other. In each column, paralleling wires were 15 mm apart from adjacent ones. Seven thermocouples were arranged near the midpoints of wires and labeled with the sequence numbers of corresponding wires.

Figure 11c illustrates the operating processes and the power consumptions of the payload with different conditions. In testing, the power source orderly energized the labeled wires with constant currents. At least 24 h interval was set between each two tests to eliminate the influence of previous tests. To compare the temperature evolutions with/without insulation layer, the bare wires #2, #3 and #6 were also energized after insulated-wire tests. Every testing procedure needed 2 h, during which the tested wire was electrified for 660 s and the CCD cameras and LED lights were turned on 15 s before electrifying the wire.

Figure 12 shows the static analysis of the payload box. The experiment apparatus was designed to be compact and operator-independent, withstanding vibration and

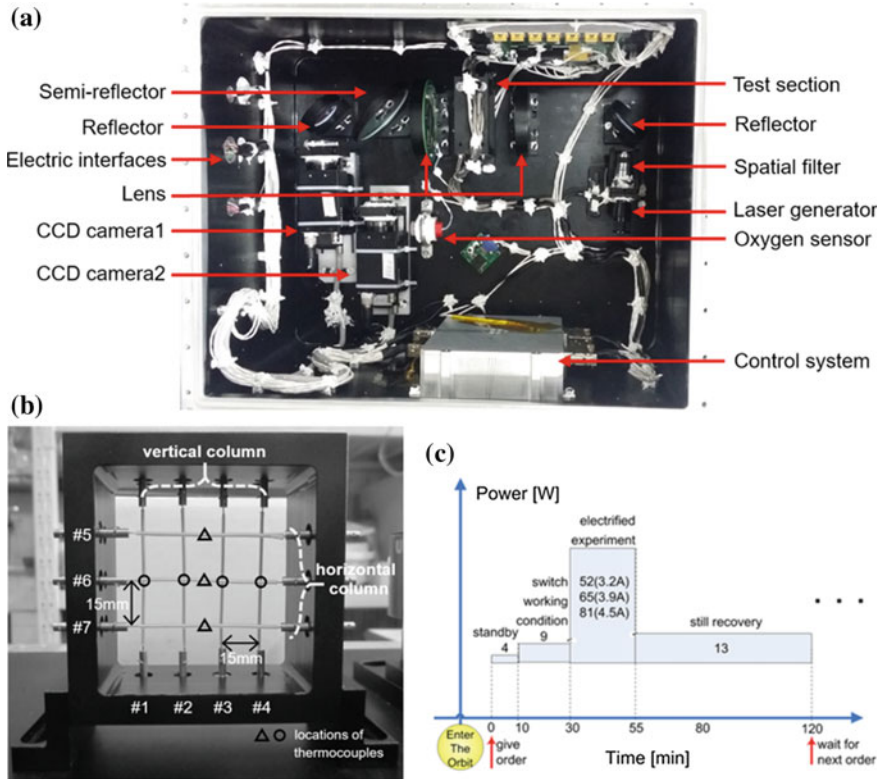


Fig. 11 a Setup of the LOWIC experimental system. b Sample configuration; triangles—the positions of thermocouples placed in horizontal column; circles—the positions of thermocouples placed in vertical column, c the operation process and power consumptions of the payload

high deceleration rate. The payload box was a $500 \times 400 \times 300$ mm rectangle vessel made of aluminum alloy, and weighted 25.5 ± 0.255 kg with all facilities. The average of total power consumption was 22.7 W and the maximum was 81 W.

5.2 Sample Selection

The tested samples are summarized in Table 5. The polyethylene (PE), though differentiated from the low flammable poly tetra fluoroethylene (PTFE, also known as Teflon) extensively used in space, was selected as the insulation material in the present study. Since the first space experiment on the wire combustion [5, 7] many researchers have extensively studied the combustion of wires using PE insulation. Such easy-melting and highly-flammable materials enable us to observe the smoke behavior of the overloaded wire safely when conducting experiment by moderate

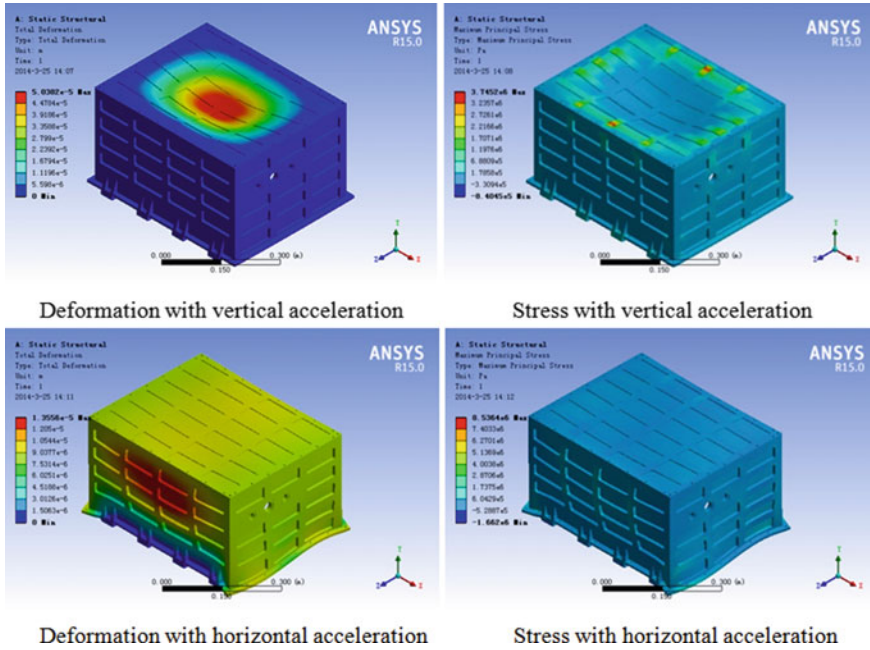


Fig. 12 Static analysis of the payload box with 90.88 m/s^2 acceleration along the Z-axis (the deformation was shown as 3000 times larger than the result)

Table 5 Parameters of the experiment

| Test | Current, A^{-1} | Thickness, mm^{-1} | Material | Wire |
|------|--------------------------|-----------------------------|----------|------|
| a | 3.2 | 0.20 | PE | #1 |
| b | 3.2 | 0.40 | PE | #2 |
| c | 3.2 | 0.50 | PE | #3 |
| d | 3.9 | 0.40 | PE | #4 |
| e | 4.5 | 0.40 | PE | #5 |
| f | 4.5 | 0.15 | PTFE | #6 |
| g | 4.5 | 0.40 | PVC | #7 |
| h | 3.2 | Non-insulated | | #2 |
| i | 3.2 | | #3 | |
| j | 4.5 | | #6 | |

current (3.2–4.5 A in this study) on the satellite. In the present study, the excess current and thickness were selected as tested parameters to further explore the characteristic of wire insulation in space.

On the ground buildings and electric devices, the less expense and easily-manufacturing of polyvinyl chloride (PVC) makes it be extensively used as insulation for electric wires. In space, the high flame resistance and low chemical activity of PTFE could expand the safe operating condition of electric wires, making it as a typical material used as insulation in spacecraft. So far, the behaviors of overloaded electric wires insulated by these two typical materials have not been compared with PE-insulated wire. In the present study, wires insulated by PVC and PTFE (wire#6 and wire#7) were tested after the PE-insulated samples to observe the smoke emitting on the surface of insulation. Wire#6 was adapted as the most commonly used sample in China's spacecraft, with 0.15 mm thickness of insulation. Wire#7 was coated by PVC insulation with a thickness of 0.4 mm, the same as the insulation thickness in test a, d, and e.

5.3 Processing of Images

The laser extinction is a commonly used fire-detection methods in space, and owing to the high-luminosity of the images captured directly, the CCD camera 2 only could make valid observation at the beginning period of smoke production. Although pyrolysis and combustion products of PE were not a single component, the laser extinction method still could be used to qualitatively record the smoke production and its following diffusing track. To simplify the computation, in this study, the component of smoke was assumed as soot, regarded as spheroids obeying the Beer-Lambert Law [48, 49]. After the data of CCD camera 1 filtered by Gauss denoising, the smoke concentration was calculated by the three-point Abel inversion. The image processing was as follows:

5.3.1 Preparation for Calculation

- Select photos before electrifying as background picture
- Get the average gray value of each background pixel
- Calculate the average gray values of the experimental pixels and those of the four subsequent pictures
- Divide the experimental values by the background values, getting the ratio picture
- Gauss denoise the ratio picture
- Normalize the ratio value of boundary, getting sharp borders of wire, flame and smoke
- Abel inverse the accumulated values in the camera direction, obtaining the smoke distribution on the cross section.

5.3.2 Calculation the Smoke Distribution

According to the Bouguers-Lambert-Beer law, the light intensity captured by camera is:

$$I = I_0 \exp\left(-\int_0^L K_e dx\right) \quad (21)$$

where I_0 is the original light intensity, and K_e represents the extinction coefficient. L is the total distance of light movement. The smoke particles are regarded as soot particles, and on this scale, the albedos and radiation emission of particles could be neglected. Therefore, K_e is equal to the absorb coefficient K_a , which could be given as:

$$K_a = \frac{\pi^2}{\lambda} E(m) N \int_0^x P(D) D^3 dD \quad (22)$$

In Eq. (22), λ is the wavelength of laser light, and m represents the complex refractive index. The refractive index m is fitted by $m = 1.755 + 0.576i$, according to $E(m)$ is given by:

$$E(m) = Im \left| \frac{m^2 - 1}{m^2 + 2} \right| \quad (23)$$

In hence, the smoke volume fraction f_v can be calculated by:

$$f_v = \frac{\pi}{6} N \int_0^x P(D) D^3 dD \quad (24)$$

where $P(D)dD$ is the occurrence possibility of particles diameters between D and $D + Dd$. After the original data filtered by Gauss denoise method, the extinction index K_e can be calculated by Abel inversion. Consequently, the smoke volume fraction is given as:

$$f_v = \frac{\lambda K_e}{6\pi E(m)}. \quad (25)$$

5.4 Smoke Emission

5.4.1 Wire with PE Insulation

Definition of Smoke Jetting Angle

Figure 13 shows the laser-illuminated images of the overloaded wires in normal gravity. It can be observed that at the end of vertical insulations, a jet angle could be observed between the insulation surface and the tangent of the high-concentration boundary. In low-pressure case, the high-concentration smoke zone expanded, and the jet angle increased from 0° to around 70° when the pressure decreased [50].

Smoke Emission at Wire Ends

Figure 14 shows the smoke emission of #1–3 wires at variable moments, with different insulation thicknesses with the same excess current. Figure 15 shows the smoke emissions of wire#4 and #5, with 3.9 A and 4.5 A current, respectively. Due to the absent buoyancy, the smoke distributing zone at two ends of the insulation were mirror-symmetrical. Such interesting space phenomenon is rarely observed on the ground where we could only gauge jet angles at the lower end of insulations. As the Fig. 14 illustrates, the high-concentration smoke zone experienced a notable shape change. Initially, the high-concentration smoke lied in a jet paralleled to the core. As time lapsing, the high-concentration smoke zone formed a half-ellipsoid surrounding the insulation end, and eventually turned into a stable shape. Meanwhile, the outer surface of insulation reached the pyrolysis temperature, and initiated smoke production. The variance of the smoke jet angle with wire#3 is shown in Fig. 16.

This process could be schematically illustrated by Fig. 17. At an early stage of overloading (0–30 s, in present study), only oxidative pyrolysis happens due to its relatively low activation energy. The heat was only supplied by the core and

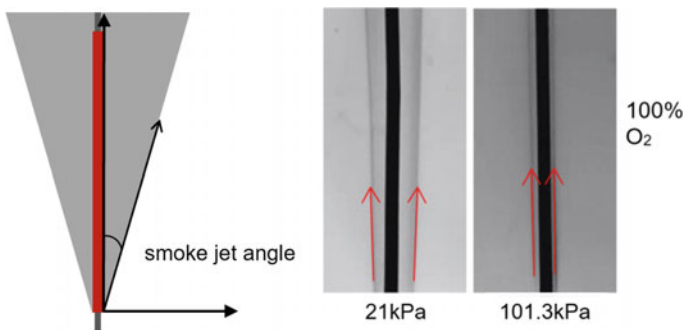


Fig. 13 Definition of the jet angle and its laser-illuminate images in normal gravity [9]

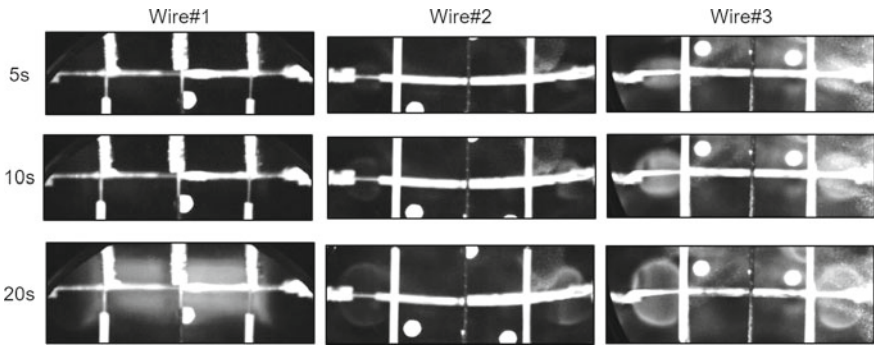


Fig. 14 Smoke emissions with different insulation thicknesses in space, wire#1–3

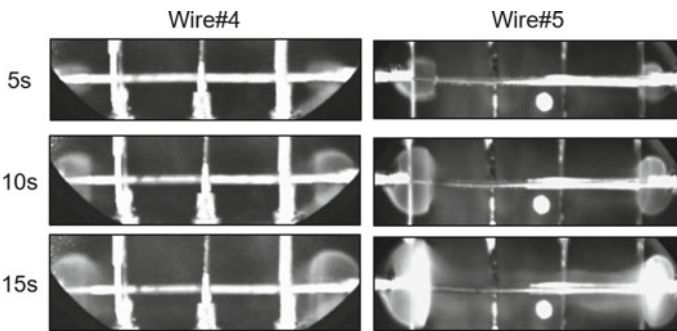


Fig. 15 Smoke emissions with different currents in space, wire#4 and #5

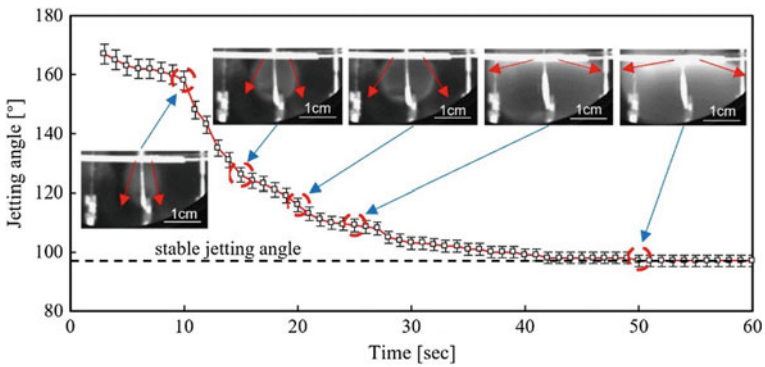


Fig. 16 Variation of the smoke jet angle with wire#3

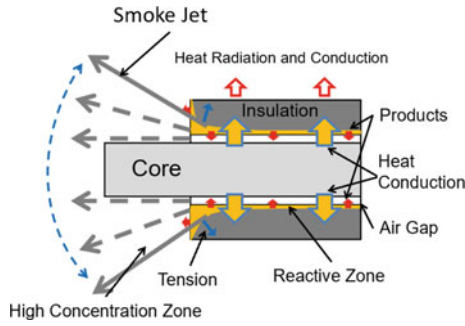


Fig. 17 Schematic illustration for the evolution of smoke jetting angle

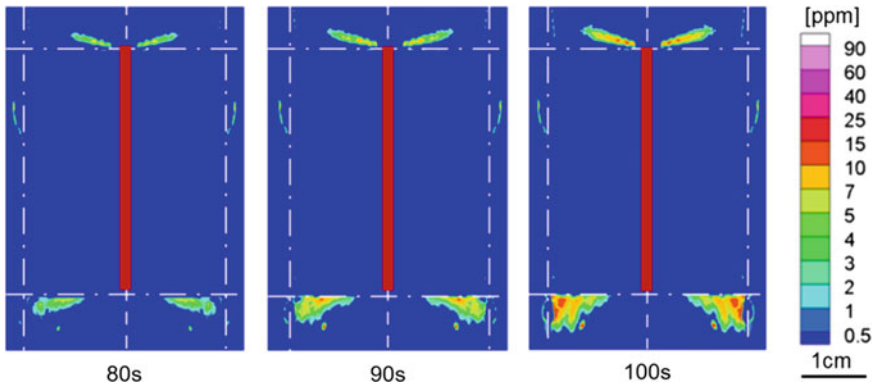


Fig. 18 Smoke distribution of the smoke jet at the ends of wire#3, computed by the laser extinction method; dotted lines—the cores; red rectangle—the insulation being tested

the reactive zone lied in the inner surface of insulation, where the PE could reach the oxygen and the core both. The pyrolysis front, located on the inner surface of swelled insulation, produced smoke escaping along the length of the wire. Then, the fuel consumption and the evolution of temperature field expanded the reactive zone. The space between the insulation end and the core was also expanded by the tension caused by the jet flow. The jet angle enlarges and eventually reached a fixed value after the reactive zone expended to the outer surface. Meanwhile, the outer insulation started to produce smoke. The insulation emitted the smoke with an unchanged morphology of the pyrolysis front. With a fixed jet angle, the smoke aggregated along the main jet, thus the CCD camera 1 could capture the smoke emission at the wire end, as Fig. 18 shows. The notable main jet constantly produces smoke till the intensive pyrolysis on the inner surface ruptures the insulation layer.

The velocities of the high-concentration smoke boundary caused by the oxidative pyrolysis from the outer surfaces of insulation were calculated. As shown in Fig. 19, the average moving rate of the high-concentration smoke boundary are in the scale of 0.3–0.5 mm/s. Smoke emission with the velocity in this scale only could be observed

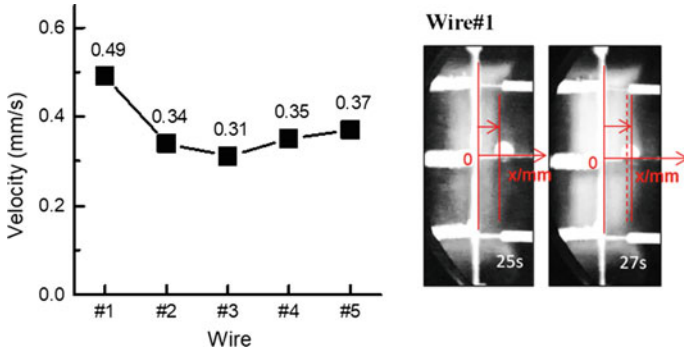


Fig. 19 Average velocity of the advancing high-concentration smoke boundary caused by reaction on the outer insulation surface in the middle of wire, 0–16 s since the beginning of the outer reaction in the case of wire#1–4, 0–14 s in the case of wire#5

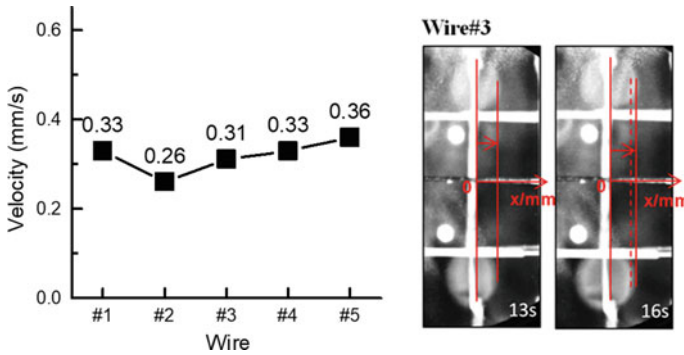


Fig. 20 Average velocities of the advancing high-concentration smoke boundary at the end of wire, 0–26 s since the beginning of end smoke jet in the case of Wire#1–4, and 0–16 s in the case of wire#5

in microgravity due to the absence of buoyancy. The velocity simply decreased with the insulation thickness and increased with the current. This velocity may be affected by many factors, such as the temperature field, the oxygen transportation etc. which requires further study in the future. Figure 20 shows the average velocity of the high-concentration boundary at the wire end moving along the direction perpendicular to the length of wire, where a same scale with the moving rate shown in Fig. 19 was found.

As shown in Fig. 21, the observable evolution of the smoke emitting stages significantly varied with the insulation thickness and the excess current. Large insulation thickness and current helped to produce visible smoke jet earlier. The evolution time of the end smoke jet became shorter with thicker insulation and larger excess current, as the stage 2 in Fig. 21 shows, indicating the end smoke jet is easier to achieve its stable state. This might be because the reactive zone is more easily to be expanded to the outer surface of insulation if the insulation is thin and the current supplies larger

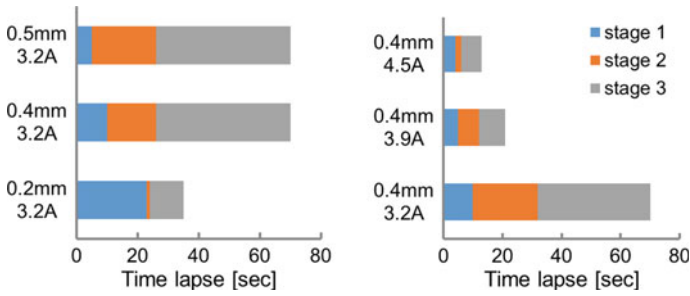


Fig. 21 Evolution of the smoke emitting stages at the wire end; stage 1—from the beginning of overload to the time the end smoke jet been captured by CCD camera 2; stage 2—from the beginning of the visible end smoke jet to the time it turned stable; stage 3—from the beginning of the stable smoke jet to the time smoke been captured by CCD camera 1

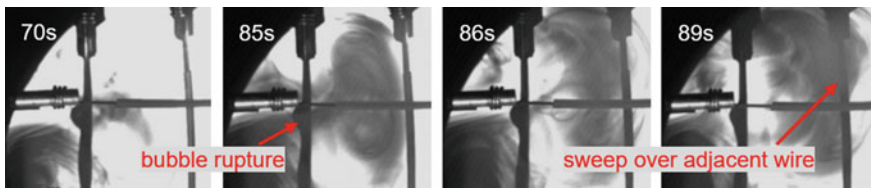


Fig. 22 Laser illuminated images of a typical bubbling jet process with wire#1

heat. Likewise, the space between the core and the insulation will be easier to be enlarged by the gas flow. In the end of stage 3, the smoke could be detected by CCD camera 1 decades second later than the end smoke emission turned stable because the laser extinction method could only observe high-concentration smoke.

Bubbling Smoke Jet

A bubbling smoke jet mode was also observed later. Caused by the heat provided by the core, the non-oxygen pyrolysis produced a bubble of smoke between the insulation layer and the core, as Fig. 22 shows. Unlike the wire end, the inner surface in middle section was isolated from the oxygen. The non-oxygen pyrolysis occurred when the temperature was high enough. The gathered smoke might raise the pressure, then, as the stress increased through smoke accumulation, there could be an insulation layer rupture. Subsequently, as the red arrow indicated, the pyrolysis product swept over the adjacent cables, showing the non-oxygen pyrolysis may cause dangerous interaction between wires. In this study, all bubbling jets happened later, after the end jets turned stable.

5.4.2 Wire with PTFE and PVC Insulations

Figure 23 shows the smoke emitting behavior of wire#6. The PTFE-insulated wire failed to achieve any intensive reaction with air in the moderate-current experiment. In the early stage of overload, the wrapping insulation produced thin smoke and detached orderly from the wire end to the middle, as Fig. 23a shows. As shown in Fig. 23b, the detachment of insulation turned slow later, creating a chance for the insulation to be sufficiently heated, where the slow rupture of the insulation occurred. After heated for 660 s, the insulation has not completely detached with the core.

Figure 24 shows the smoke emission of wire#7. The PVC-insulated wire produced heavy smoke with 4.5 A current. As shown in Fig. 24a, the concentration of smoke was much higher than that of wire#6. Afterwards, the high-concentration zone of smoke lost its symmetry within 10 s, as illustrated in Fig. 24b. An intensive smoke jet emerged and created strong disturbance of the ambient environment. After 660 s overload, the PVC insulation remained a bulged remnants around the metallic core.

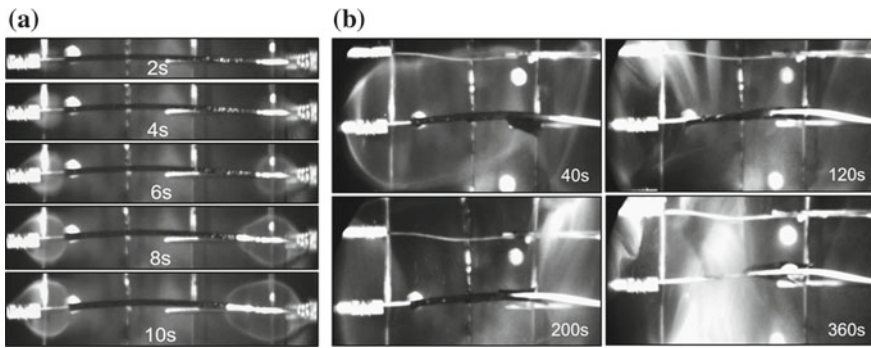


Fig. 23 a Symmetrical smoke emission and ordered detachment of PTFE insulation in early stage. b Slow rupture of PTFE insulation in late stage

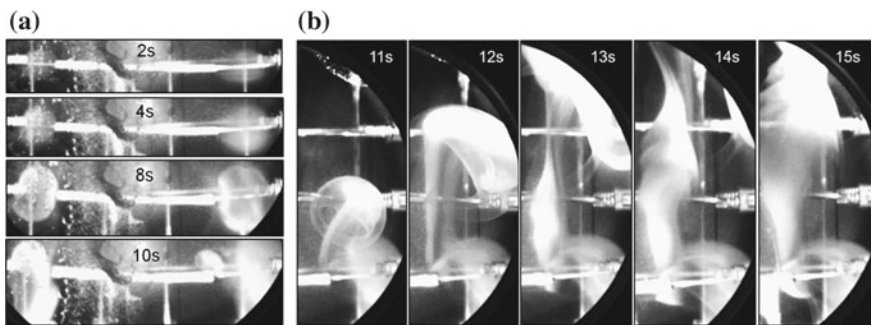


Fig. 24 a Symmetrical smoke emission of PTFE insulation in early stage. b Asymmetrical smoke jet of PTFE insulation at the wire end

5.5 Temperature Variation

5.5.1 Simplified Model

A simplified model is applied to describe the temperature rise of wire. When overloaded, the constant current will heat the wire up. The temperature of wire rises and will eventually reach a nearly steady-state value. Only heat transfer occurs before any reaction starts.

Other assumptions are made as follows:

- (1) The temperature field of the wire is uniform and thermally-thin theory is applied.
- (2) The wire is long and the heat was conducted only along the radial direction.
- (3) Through the whole process, all thermal properties and the electric resistance of wire are constant.
- (4) All parameters of the ambient medium are constant.

The energy equation is:

$$mc \frac{dT}{dt} = I^2 R - KA(T - T_0) \tag{26}$$

where m , A , and R are the mass, area of outer surface and electric resistance of wire per unit length, with the specific heat capacity c . The integrated heat transfer coefficient on the outer surface is K . On the ground, the heat transfer coefficient K depends on many factors, such as the natural convection, forced convection, heat conduction, and thermal radiation. T and T_0 represent the temperatures of wire and ambient environment respectively. The time since the overload is t . Therefore we get excess temperature as:

$$\theta = T - T_0 = \frac{I^2 R}{KA} \left(1 - \exp\left(-\frac{KA t}{mc}\right) \right) + (T_1 - T_0) \exp\left(-\frac{KA t}{mc}\right) \tag{27}$$

where T_1 is the initial temperature of wire, and set $\theta_\infty = \frac{I^2 R}{KA}$, $\theta_0 = T_1 - T_0$, $t_m = \frac{mc}{KA}$, thus we get:

$$\theta = \theta_\infty \left(1 - \exp\left(-\frac{t}{t_m}\right) \right) + \theta_0 \exp\left(-\frac{t}{t_m}\right) \tag{28}$$

For the temperature rising rate f :

$$f = \frac{d\theta}{dt} = \frac{\theta_\infty - \theta_0}{t_m} \exp\left(-\frac{t}{t_m}\right) = \frac{I^2 R - \theta_0 KA}{mc} \exp\left(-\frac{KA t}{mc}\right) \tag{29}$$

Therefore if the wire undergoes different excess currents, we get:

$$\frac{\partial f}{\partial I} = \frac{2RI}{mc} \exp\left(-\frac{KAt}{mc}\right) \tag{30}$$

And the temperature rising rate changes with the integrated heat transfer coefficient as:

$$\frac{\partial f}{\partial K} = \frac{-(\theta_0 Amc + (\theta_\infty - \theta_0)KA^2t)}{(mc)^2} \exp\left(-\frac{KAt}{mc}\right) \tag{31}$$

We can easily find the temperature rising rate increases with the excess current I while decrease with the integrated heat transfer coefficient K on the outer surface of wire. Though in actual pre-ignition scenarios, the heat transfer is much more complicated than the model demonstrated above, it helps us predict the tendency of the temperature when the condition changes.

Figure 25 shows the temperature records when wire#2 and wire#3 is electrified and provides comparison with the bare-wire tests. Instead of monotonically rising as the bar-wire temperature did, the temperatures of insulated wires showed transient fluctuations. The integrated heat transfer coefficient K in Eq. (9) changed here, and the current I remained constant through the overload. Other thermocouples also recorded similar fluctuations, showing the temperature fluctuations were not caused by the thermal expansion of heated core.

5.5.2 Confirmation of Bubbling Jet

A one-dimension analysis of heat transfer could help analyze the temperature fluctuations further. As Figure 25 shows, in the tests of wire#2 and #3, the fluctuations

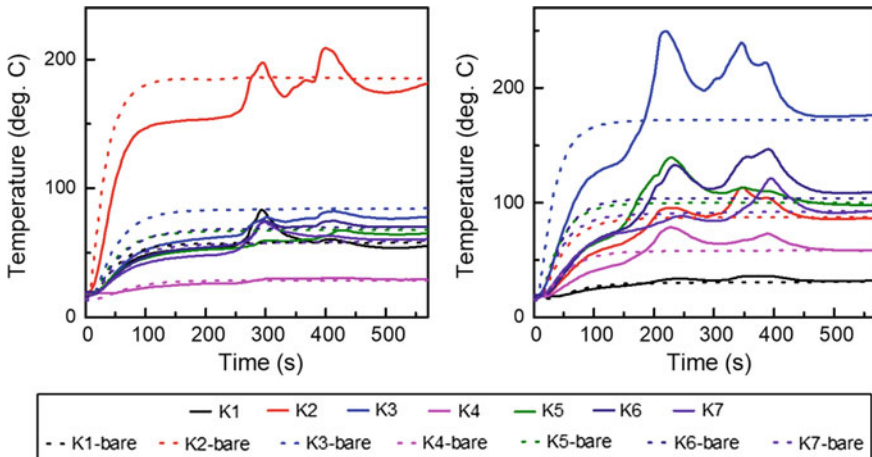


Fig. 25 The temperature records in insulated/bare wire tests, with 3.2 A current

occurred later than the temperatures in bare-wire tests reached a steady state. In steady-state heat transfer, the temperature of metallic core maintained constant (when the temperature rising rate was less than 0.1 °C/s, set in the present study), the heat was conducted through the insulation layer with a constant heat flux per unit time. Before any insulation rupture or bubble smoke jet occurred, the insulation still acted as a heat conductor. Here we get:

$$q = \frac{T_i - T_0}{R_{tm}} = const \tag{32}$$

where q is the heat supplied by the core per unit length, and R_{tm} is the thermal resistance per unit length of the media between the core and the thermocouples. T_i is the temperatures on the inner surface of insulation, and T_0 is the value recorded by thermocouple. For the thermal resistance, we get:

$$R_{tm} = \frac{1}{2\pi\lambda_{pe}} \ln\left(\frac{d_i + \delta}{d_i}\right) + \frac{1}{2\pi\lambda_{air}} \ln\left(\frac{d_o}{d_i + \delta}\right) \tag{33}$$

where λ_{pe} and λ_{air} are the thermal conductivities of PE and air respectively. d_i is the diameter of the core and δ is the insulation thickness. d_o indicates the distance from the thermocouple to the center axis of core. Usually, λ_{pe} is almost ten times larger than λ_{air} . The temperature records of insulated tests should be higher than those in bare-wire tests. Before temperature fluctuating, the present study recorded lower temperatures with insulations than those with bare cores. This implies the heat was not totally conducted to the outer surface of insulation and some amount of it may be consumed by temperature rising, phase transition and pyrolysis of the insulation. When the fluctuation occurred, thermocouples even recorded higher temperatures than in bare-wire tests, reflecting the high temperatures of insulation debris and pyrolysis products inside the insulation layer.

5.5.3 Typical Temperature Evolutions of PE-Insulated Wires

Compared with bare-wire tests, the temperature history of PE-insulated wire could be summarized into three stages:

- (1) In the early stage, the insulation layer acted as a heat insulator, slowing down the temperature rise recorded by the thermocouple. According to Eq. (9), since the mc of PE is higher than that of air, the existence of insulation decreased the temperature rising rate f and therefore made the temperature rise more slowly than that of bare wire.
- (2) In the middle stage, temperature fluctuations occurred due to the bursting high-temperature smoke and the rupture of insulation. The pyrolysis products and insulation debris caused fluctuating temperatures which were even higher than those in the bare-wire tests.

- (3) In the late stage, when the degradation of insulation completed, the temperature records reached the balance values, which were nearly the same as those in bare-wire tests.

5.5.4 Effect of Thickness on PE Insulation

Figure 26 shows the temperature histories of wire#1–3 in normal gravity and microgravity. In microgravity, the temperatures rose faster and achieved a higher steady-state value. The temperature histories show more different when the insulation thickness changed. In 0–80 s, the temperatures increase less with thicker insulations. This may be because the larger mc of PE decrease the f in Eq. (29). Besides, the temperature fluctuated more times with thicker insulation, showing times of bubbling smoke jets were needed to completely rupture the insulation.

The first peaks of fluctuations with 0.2 mm, 0.4 mm and 0.5 mm came in 111 s, 294 s, and 219 s respectively, indicating there may be a tradeoff between the smoke production and the stress tension on the inner surface of insulation. The maximum temperature increases with insulation thickness. It may be because higher tension the insulation could undergo made it possible to form high-temperature and high-pressure smoke inside the bubble.

5.5.5 Effect of Current on PE Insulation

Figure 27 illustrates the temperature histories of 0.4 mm PE-insulated wires with different current. In normal gravity, though with different current, the temperature histories fail to show notable differences since the thickness of the natural convection boundary very thin and its cooling effect became stronger when the density

Fig. 26 The temperature histories of the wire#1–3, electrified by 3.2 A current

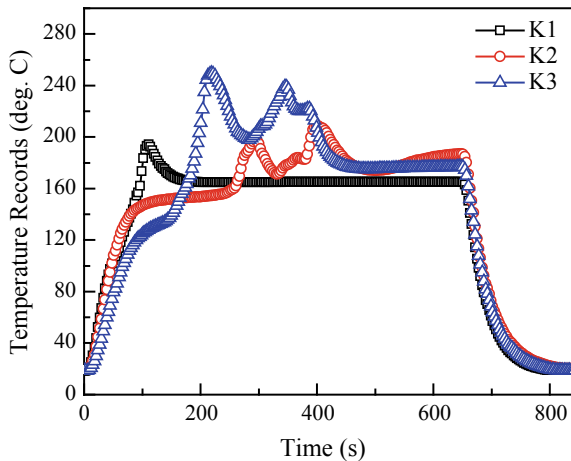
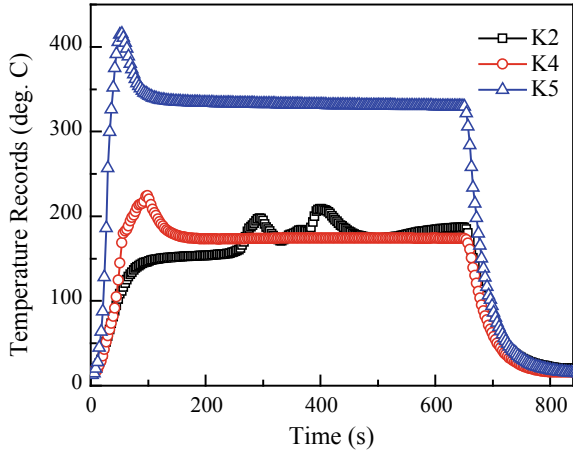


Fig. 27 The temperature histories of the wires#2, 4, and 5, with 0.4 mm insulation



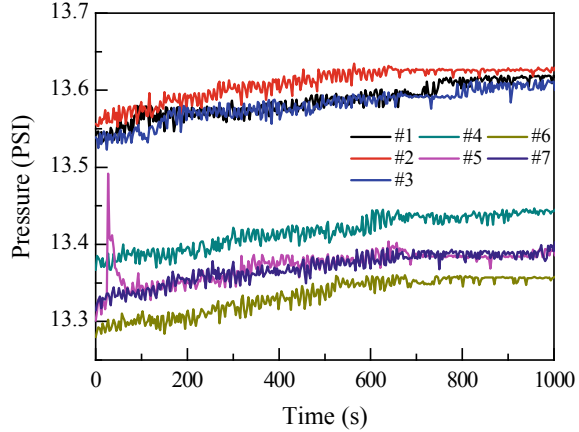
difference of ambient air became larger. In microgravity, the temperature rises with different current could be easily differentiated with each other. In the early stage, the temperature rising rate significantly increased with the current. It showed the similar tendency as the Eq. (30). The first peaks of temperature fluctuations also came earlier with larger current.

The extents of overheat, defined as the differences between the local extreme temperature and the balanced temperature, could measure the additional temperature rise caused by burst pyrolysis products and hot insulation debris. The overheat extent increased from 28 °C to 85 °C when the current increased from 3.2 to 4.5 A, implying hotter smoke inside the bubble with larger current. The frequency of fluctuation decreased with the current and the peak of it became sharper. This may showed that with large current, stronger smoke production and less bubbling jets needed to rupture the insulation layer. The 4.5 A excess current managed to induce a stable and visible flame, whereas only flash were observed in other tests. We should note that after the intensive rupture of wire, the cores were usually inevitable bent, which was caused by the heat and the strong insulation rupture. This bending will change the distance between the wire and its thermocouple, bringing detecting errors.

5.6 Environment Parameters

Figure 28 shows the variation of pressure inside the payload box when testing samples. When electrifying the tested wire, the heat supplied by current heated the air up and produced gaseous products of pyrolysis, leading to higher records of the pressure sensor. After all tests, the ambient pressure decreased by less than 0.3PSI. Figure 29 illustrates the relative concentration of oxygen during the tests. The wire#5 achieved to sustain a visible flame in the early stage of overload, both the pressure and oxygen

Fig. 28 The pressure inside the payload box during tests

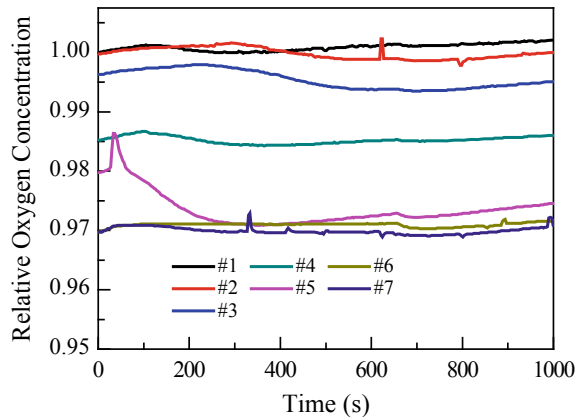


records abruptly increased and subsequently decreased at that time. When the experiment ended, the oxygen concentration decreased by less than 0.0035 mol fraction in total, lying in the permitted range of error

5.7 Conclusions of SJ-10 Experiments

In the space experiment, the smoke emission of the overloaded wire was investigated in long-term microgravity for the first time. The smoke emission firstly started in wire ends, decades second before the temperature record reached a balanced value. The evolution of the high-concentration smoke zone showed the geometry of pyrolysis front dominated the direction of end smoke jet. The laser extinction method detected

Fig. 29 The relative oxygen records inside the payload box during tests, setting the oxygen record before any test as 1.0



the end smoke jet until the jet boundary reached a stable angle and the smoke accumulated along a main jet. In the middle wire section, bubbling smoke jets occurred and caused fluctuations of temperature records when rupturing the insulation. The bubbling smoke jet may be attributed to the non-oxygen pyrolysis on the inner surface. It produced high-temperature smoke that eventually burst out from the melt insulation. The smoke emission of overloaded wire with PVC and PTFE insulation were observed. The wrapping PTFE insulation was orderly detached from the metallic core when overload, without intensive smoke emission. The high-concentration zone of smoke at the end of PVC-insulated wire lost its symmetry within 10 s and created a heavy smoke jet.

The temperature records also showed unique phenomena in microgravity and also helped to confirm the bubbling smoke jet with PE insulation. In the early stage, the temperature rose slowly with thicker insulation. When thicker insulation being ruptured, the stronger and more frequent temperature fluctuations were observed. With a larger current, the fluctuations came earlier and with sharper fluctuating peaks. The fluctuation times decreased under the similar condition, indicating the insulation was ruptured faster and more completely.

References

1. Robert F (1994) Risks and issues in fire safety on the space station, NASA TM-106430
2. Friedman R (1998) Fire safety in extraterrestrial environments. NASA TM-207417
3. Limero T, Wilson S, Perlot S, James J (1992) The role of environmental health system air quality monitors in space station contingency operations. SAE Trans 101:1521
4. Babrauskas V (2003) Information on specific materials and devices. In: Babrauskas V (ed) Ignition handbook: principles and applications to fire safety engineering, fire investigation, risk management and forensic science. Fire Science Publishers, Issaquah, pp 774–795
5. Greenberg PS, Sacksteder KR, Kashiwagi T (1994) Wire insulation flammability experiment: USML-1 1 Year post mission summary. NASA CP 3272 2, p 631
6. Thomas HC, Donald AP 1971 Burning of Teflon-insulated wires in supercritical oxygen at normal and zero gravities. NASA TM-2174
7. Greenberg PS, Sacksteder KR, Kashiwagi T (1995) Wire insulation flammability. NASA CP 10174, p 25
8. Kikuchi M, Fujita O, Ito K, Sato A, Sakuraya T (1998) Experimental study on flame spread over wire insulation in microgravity. Proc Combust Inst 27:2507
9. Kikuchi M, Fujita O, Ito K, Sato A, Sakuraya T (2000) Flame spread over polymeric wire insulation in microgravity. Space Forum 6:245
10. Fujita O, Kikuchi M, Ito K, Nish K (2000) Effective mechanisms to determine flame spread rate over thylene-tetrafluoroethylene wire insulation: discussion on dilution gas effect based on temperature measurements. Proc Combust Inst 28:2905
11. Fujita O, Nish K, Ito K (2002) Effect of low external flow on flame spread over polyethylene-insulated wire in microgravity. Proc Combust Inst 29:2545
12. Umem A, Uchi M, Hira T (2002) Physical model analysis of flame spreading along an electrical wire in microgravity. Proc Combust Inst 29:2535–2543
13. Kong WJ, Lao SQ, Zhang PY (2006) Study on wire insulation flammability at microgravity by functional simulation method. J Combust Sci Technol 12(1):1–4
14. Chen LF, Xin Z, Kong WJ (2006) Functional simulations of the fire precursor of the wire insulation in quiescent microgravity environment. Chin J Space Sci 26(3):235–240

15. Kong WJ, Wang BR, Law SQ (2007) Study on fire precursor of wire insulation in low-pressure environments. *J Eng Thermophys* 28(6):1047–1049
16. Kong WJ, Wang BR, Zhang WK (2008) Study on prefire phenomena of wire insulation in microgravity. *Microgravity Sci Technol* 20:107–113
17. Nakamura Y, Yoshimura N, Matsumura T et al (2008) Flame spread over polymer-insulated wire in sub-atmospheric pressure: similarity to microgravity phenomena. *Prog Scale Model*, 17–27
18. Nakamura Y, Yoshimura N, Ito H et al (2009) Flame spread over electric wire in sub-atmospheric pressure. *Proc Combust Inst* 32:2559–2566
19. Fujita O, Kyono T, Kido Y (2011) Ignition of wire insulation with short-term excess electric current in microgravity. *Proc Combust Inst* 33(2):2617–2623
20. Takano Y, Fujita O, Shigeta N (2013) Ignition limits of short-term overloaded electric wires in microgravity. *Proc Combust Inst* 34(2):2665–2673
21. Takahashi S, Ito H, Nakamura Y, Fujita O (2013) Extinction limits of spreading flames over wires in microgravity. *Combust Flame* 160:1900–1902
22. Takahashi S, Takeuchi H, Ito H, Nakamura Y, Fujita O (2013) Study on unsteady molten insulation volume change during flame spreading over wire insulation in microgravity. *Proc Combust Inst* 34(2):2657–2664
23. Osorio AF, Mizutani K, Fernandez-Pello C, Fujita O (2015) Microgravity flammability limits of ETFE insulated wires exposed to external radiation. *Proc Combust Inst* 35:2683–2689
24. Hu LH, Zhang YS, Yoshioka K et al (2015) Flame spread over electric wire with high thermal conductivity metal core at different inclinations. *Proc Combust Inst* 35(3):2607–2614
25. Fujita O (2015) Solid combustion research in microgravity as a basis of fire safety in space. *Proc Combust Inst* 35(3):2487–2502
26. Hu WR, Zhao JF, Long M, Zhang XW, Liu QS, Hou MY, Kang Q, Wang YR, Xu SH, Kong WJ, Zhang H, Wang SF, Sun YQ, Hang HY, Huang YP, Cai WM, Zhao Y, Dai JW, Zheng HQ, Duan EK, Wang JF (2014) Space program SJ-10 of microgravity research. *Microgravity Sci Technol* 26:159–169
27. Xue S, Kong W (2019) Smoke emission and temperature characteristic of the long-term overloaded wire in space. *J Fire Sci* 37(2): 99–116
28. Xue S, Kong W (2018) Overload characteristic of typical electric wire insulation material in microgravity. In: Keynote lecture, 12th Asian microgravity symposium, Zhuhai, China, 12–16 November 2018
29. Ivanov AV, Balashov YV (1999) Experimental verification of material flammability in space. NASA/CR-1999-209405
30. Zik O, Olami Z, Moses E (1998) Fingering instability in combustion. *Phys Rev Lett* 81(18):3868–3871
31. Zik O, Olami Z, Moses E (1998) Fingering instability in solid fuel combustion: the characteristic scales of the developed state. The Combustion Institute, pp 2815–2830
32. Wichman IS, Olson SL (2003) Flamelet formation in hele-shaw flow. NASA/CP-2003-212376/REV1, pp 29–31
33. Olson SL, Miller FJ, Jahangirian S, Wichman IS (2009) Flame spread over thin fuels in actual and simulated microgravity conditions. *Combust Flame* 2009:1214–1226
34. Zhang X (2007) Simulation of flame spread over thin solid fuel under microgravity using narrow channel on ground. *Chin J Theor Appl Mech* 39(4):466–472
35. Zhang X (2008) Opposed-flow flame spread over a thin solid material in narrow channels in normal and microgravity. *J Eng Thermophys* 29(2):347–350
36. Zhang X, Yu Y (2008) Comparability of flame spread over thin solid fuel surface under different gravities. *J Combust Sci Technol* 14(4):289–294
37. Xiao Y, Hu J, Wang SF (2010) A narrow channel experimental study on flammability characteristics of thermally thin fuels under simulated microgravity conditions. *J Astronaut* 31(7):1877–1882
38. Wang K, Wang BR, Ai YH, Kong WJ (2012) Study on the pre-ignition characteristics of wire insulation in the narrow channel setup. *Sci China Technol Sci* 55:2132–2139

39. Xiao Y, Ren T, Wang SF (2010) Flame spread over thermally thick fuels in narrow channel apparatus. *J Eng Thermophys* 31(8):1423–1426
40. Wang K, Ai YH, Wang BR, Kong WJ (2012) Study on pre-fire characteristics of wire insulation by overload in weakly buoyant environment. *J Eng Thermophys* 33(4):689–693
41. Wang K, Wang BR, Kong WJ, Liu FS (2014) Study on the pre-ignition temperature variations of wire insulation under overload conditions in microgravity by the functional simulation method. *J Fire Sci* 32(3):257–280
42. Bergman TL, Lavine AS, Incropera FP (2011) *Fundamentals of heat and mass transfer*, 7th edn. Wiley, Jefferson City, USA
43. Gebhart B, Jaluria Y, Mahajan RL, Sammakia B (1988) *Buoyancy-induced flows and transport*. Hemisphere, Washington, DC
44. Hu WR, Tang BC (2017) Kang Q progress of microgravity experimental satellite SJ-10. *Aeron Aero Open Access J* 1(3):00016
45. Zhao HG, Qiu JW, Tang BC et al (2016) The SJ-10 recoverable microgravity satellite of China. *J Space Explor* 5(1):101
46. Wang Y, Zhao H, Zhang Y et al (2016) Establishing and evaluation of the microgravity level in the SJ-10 recoverable satellite. *Aeros China* 17(4):3–13
47. Kong WJ, Wang BR, Xia W (2016) Experimental facility for wire insulation combustion in SJ-10. *Physics* 45(4):219–224
48. Greenberg PS, Ku JC (1997) Soot volume fraction imaging. *Appl Opt* 36(22):5514–5522
49. Iuliis SD, Barbini M, Benecchi S et al (1998) Determination of the soot volume fraction in an ethylene diffusion flame by multiwavelength analysis of soot radiation. *Combust Flame* 115(s1–2):253–261
50. Xia W, Wang K, Wang BR et al (2016) Study on combustion characteristics of overloaded wire insulation at the early stage of fire in weak buoyancy. *J Eng Thermophys* 37(4):876–882